Republic of Indonesia

Indonesia Climate Change Sectoral Roadmap
ICCSR

Scientific Basis:
Analysis and Projection of Sea Level Rise and Extreme Weather Event

March 2010

AUTHORS

Indonesia Climate Change Sectoral Roadmap - ICCSR

Scientific basis: Analysis and Projection of Sea Level Rise and Extreme Weather Events

Adviser

Prof. Armida S. Alisjahbana, Minister of National Development Planning/Head of Bappenas

Editor in Chief

U. Hayati Triastuti, Deputy Minister for Natural Resources and Environment, Bappenas

ICCSR Coordinator

Edi Effendi Tedjakusuma, Director of Environmental Affairs, Bappenas

Editors

Irving Mintzer, Syamsidar Thamrin, Heiner von Luepke, Dieter Brulez

Synthesis Report

Coordinating Authors for Adaptation: Djoko Santoso Abi Suroso

Scientific Basis: Analysis and Projection Sea Level Rise and Extreme Weather Event Report

Author: Ibnu Sofian

Technical Supporting Team

Chandra Panjiwibowo, Edi Riawan, Hendra Julianto, Leyla Stender, Tom Harrison, Ursula Flossmann-Krauss

Administrative Team

Altamy Chrysan Arasty, Risnawati, Rinanda Ratna Putri, Siwi Handinah, Wahyu Hidayat, Eko Supriyatno, Rama Ruchyama, Arlette Naomi, Maika Nurhayati, Rachman

ACKNOWLEDGMENTS

The Indonesia Climate Change Sectoral Roadmap (ICCSR) is meant to provide inputs for the next five year Medium-term Development Plan (RPJM) 2010-2014, and also for the subsequent RPJMN until 2030, laying particular emphasis on the challenges emerging in the forestry, energy, industry, agriculture, transportation, coastal area, water, waste and health sectors. It is Bappenas policy to address these challenges and opportunities through effective development planning and coordination of the work of all line ministries, departments and agencies of the Government of Indonesia (GoI). It is a dynamic document and it will be improved based on the needs and challenges to cope with climate change in the future. Changes and adjustments to this document would be carried out through participative consultation among stakeholders.

High appreciation goes to Mrs. Armida S. Alisyahbana as Minister of National Development Planning /Head of the National Development Planning Agency (Bappenas) for the support and encouragement. Besides, Mr. Paskah Suzetta as the Previous Minister of National Development Planning/ Head of Bappenas who initiated and supported the development of the ICCSR, and Deputy Minister for Natural Resources and Environment, Ministry of National Development Planning /Bappenas, who initiates and coordinates the development of the ICCSR.

To the following steering committee, working groups, and stakeholders, who provide valuable comments and inputs in the development of the ICCSR Scientific basis for Analysis and Projection Sea Level Rise and Extreme Weather Events document, their contributions are highly appreciated and acknowledged:

Steering Committee (SC)

Deputy of International Cooperation, Coordinating Ministry for Economy; Secretary of Minister, Coordinating Ministry for Public Welfare; Executive Secretary, Agency for Meteorology, Climatology; Deputy of Economy, Deputy of Infrastructures, Deputy of Development Funding, Deputy of Human Resources and Culture, Deputy of Regional Development and Local Autonomy, National Development Planning Agency; and Chief of Secretariat of the National Council for Climate Change.

Working Group

National Development Planning Agency

Sriyanti, Yahya R. Hidayat, Bambang Prihartono, Mesdin Kornelis Simarmata, Arum Atmawikarta, Montty Girianna, Wahyuningsih Darajati, Basah Hernowo, M. Donny Azdan, Budi Hidayat, Anwar Sunari, Hanan Nugroho, Jadhie Ardajat, Hadiat, Arif Haryana, Tommy Hermawan, Suwarno, Erik Amundito, Rizal Primana, Nur H. Rahayu, Pungki Widiaryanto, Maraita, Wijaya Wardhana, Rachmat Mulyanda, Andiyanto Haryoko, Petrus Sumarsono, Maliki

Agency for Meteorology, Climatology and Geophysics

Edvin Aldrian, Dodo Gunawan, Nurhayati, Soetamto, Yunus S, Sunaryo

National Institute of Aeuronatics and Space

Agus Hidayat, Halimurrahman, Bambang Siswanto, Erna Sri A, Husni Nasution

Research and Implementatiton of Technology Board

Eddy Supriyono, Fadli Syamsuddin, Alvini, Edie P

National Coordinating Agency for Survey and Mapping

Suwahyono, Habib Subagio, Agus Santoso

Grateful thanks to all staff of the Deputy Minister for Natural Resources and Environment, Ministry of National Development Planning/ Bappenas, who were always ready to assist the technical facilitation as well as in administrative matters for the finalization process of this document.

The development of the ICCSR document was supported by the Deutsche Gesellschaft für Technische Zusammenarbeit (GTZ) through its Study and Expert Fund for Advisory Services in Climate Protection and its support is gratefully acknowledged.

Remarks from Minister of National Development Planning/ Head of Bappenas

We have seen that with its far reaching impact on the world's ecosystems as well as human security and development, climate change has emerged as one of the most intensely critical issues that deserve the attention of the world's policy makers. The main theme is to avoid an increase in global average temperature that exceeds 2°C, i.e. to reduce annual worldwide emissions more than half from the present level in 2050. We believe that this effort of course requires concerted international response – collective actions to address potential conflicting national and international policy initiatives. As the world economy is now facing a recovery and developing countries are struggling to fulfill basic needs for their population, climate change exposes the world population to exacerbated life. It is necessary, therefore, to incorporate measures to address climate change as a core concern and mainstream in sustainable development policy agenda.

We are aware that climate change has been researched and discussed the world over. Solutions have been proffered, programs funded and partnerships embraced. Despite this, carbon emissions continue to increase in both developed and developing countries. Due to its geographical location, Indonesia's vulnerability to climate change cannot be underplayed. We stand to experience significant losses. We will face – indeed we are seeing the impact of some these issues right now- prolonged droughts, flooding and increased frequency of extreme weather events. Our rich biodiversity is at risk as well.

Those who would seek to silence debate on this issue or delay in engagement to solve it are now marginalized to the edges of what science would tell us. Decades of research, analysis and emerging environmental evidence tell us that far from being merely just an environmental issue, climate change will touch every aspect of our life as a nation and as individuals.

Regrettably, we cannot prevent or escape some negative impacts of climate change. We and in particular the developed world, have been warming the world for too long. We have to prepare therefore to adapt to the changes we will face and also ready, with our full energy, to mitigate against further change. We have ratified the Kyoto Protocol early and guided and contributed to world debate, through hosting the 13th Convention of the Parties to the United Nations Framework Convention on Climate Change (UNFCCC), which generated the Bali Action Plan in 2007. Most recently, we have turned our attention to our biggest challenge yet, that of delivering on our President's promise to reduce carbon emissions by 26% by 2020. Real action is urgent. But before action, we need to come up with careful analysis, strategic planning and priority setting.

I am delighted therefore to deliver *Indonesia Climate Change Sectoral Roadmap,* or I call it ICCSR, with the aim at mainstreaming climate change into our national medium-term development plan.

The ICCSR outlines our strategic vision that places particular emphasis on the challenges emerging in the forestry, energy, industry, transport, agriculture, coastal areas, water, waste and health sectors. The content of the roadmap has been formulated through a rigorius analysis. We have undertaken vulnerability assessments, prioritized actions including capacity-building and response strategies, completed by associated financial assessments and sought to develop a coherent plan that could be supported by line Ministries and relevant strategic partners and donors.

I launched ICCSR to you and I invite for your commitment support and partnership in joining us in realising priorities for climate-resilient sustainable development while protecting our population from further vulnerability.

Minister for National Development Planning/

Head of National Development Planning Agency

Prof. Armida S. Alisjahbana

Remarks from Deputy Minister for Natural Resources and Environment, Bappenas

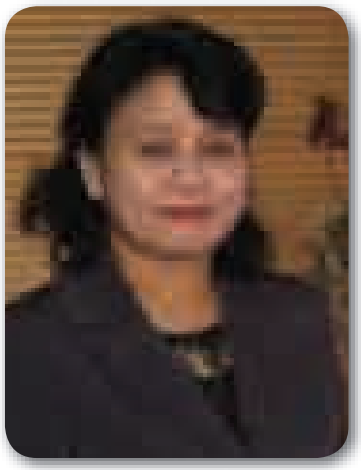

To be a part of the solution to global climate change, the government of Indonesia has endorsed a commitment to reduce the country's GHG emission by 26%, within ten years and with national resources, benchmarked to the emission level from a business as usual and, up to 41% emission reductions can be achieved with international support to our mitigation efforts. The top two sectors that contribute to the country's emissions are forestry and energy sector, mainly emissions from deforestation and by power plants, which is in part due to the fuel used, i.e., oil and coal, and part of our high energy intensity.

With a unique set of geographical location, among countries on the Earth we are at most vulnerable to the negative impacts of climate change. Measures are needed to protect our people from the adverse effect of sea level rise, flood, greater variability of rainfall, and other predicted impacts. Unless adaptive measures are taken, prediction tells us that a large fraction of Indonesia could experience freshwater scarcity, declining crop yields, and vanishing habitats for coastal communities and ecosystem.

National actions are needed both to mitigate the global climate change and to identify climate change adaptation measures. This is the ultimate objective of the *Indonesia Climate Change Sectoral Roadmap*, ICCSR. A set of highest priorities of the actions are to be integrated into our system of national development planning. We have therefore been working to build national concensus and understanding of climate change response options. The *Indonesia Climate Change Sectoral Roadmap* (ICCSR) represents our long-term commitment to emission reduction and adaptation measures and it shows our ongoing, inovative climate mitigation and adaptation programs for the decades to come.

Deputy Minister for Natural Resources and Environment

National Development Planning Agency

U. Hayati Triastuti

LIST OF CONTENTS

AUTHORS i

ACKNOWLEDGMENTS iii

Remarks from Minister of National Development Planning/Head of Bappenas v

Remarks from Deputy Minister for Natural Resources and Environment, Bappenas vii

LIST OF TABLES x

LIST OF FIGURES xi

LIST OF ABBREVIATIONS xv

1 INTRODUCTION 1

1.1 Background 2

1.2 Aims and Objectives 3

2 CLIMATE AND OCEANOGRAPHIC CONDITION IN INDONESIAN SEAS 5 2.1 Wind and Rain Patterns 6

2.2 Sea Level Variations 7

2.2.1 Ocean Currents and Sea Level 7

2.2.2 Tidal Forcing 10

2.2.3 Significant Wave Height 11

2.3 The Distribution of Chlorophyll-a and Sea Surface Temperature 12

3 METHODOLOGY 15

3.1 Data 16

3.2 Method 17

4 PROJECTION OF SEA LEVEL RISE AND SEA SURFACE TEMPERATURE 23

4.1 Sea Surface Temperature Rise Projection 24

4.2 Sea Level Rise Projection 28

4.2.1 Sea Level Rise Projection based on the IPCC AR4 28

4.2.2 Sea Level Rise Projection (Post-IPCC AR4) 33

5 EL NIÑO AND LA NIÑA PROJECTIONS 39

5.1 Global Warming and ENSO 41

5.2 ENSO and Sea Level Variations 45

5.2.1 ENSO and Mean Sea level 45

5.2.2 ENSO and Extreme Waves 47

5.3 ENSO, Sea Surface Temperature and Chlorophyll-a 51

5.4 ENSO and Coral Bleaching 53

6 ESTIMATION OF INUNDATED AREA 57

6.1 Inundated Area Estimation 58

6.2 Inundated Area Estimation during Extreme Weather Events 61

CHAPTER 7 CONCLUSIONS AND RECOMMENDATIONS 68

REFERENCES 69

LIST OF TABLES

Table 4. 1 Projection of the SST increase of Indonesian waters 27

Table 4. 2 Potential source of the sea level rise 27

Table 4. 3 Projection of the average increase of sea level in Indonesian waters 33

Table 5. 1 ENSO timetable based on MRI model output 45

LIST OF FIGURES

Figure 1. 1	Flow chart of climate change study in support to climate change adaptation action plan	3
Figure 2. 1	The pattern of wind and sea level temperature (SLT) on January and August	7
Figure 2. 2	Annual cycle of mean rainfall in Indonesia on January and August	7
Figure 2. 3	Spatial distribution of SLH and surface current on January and August.	8
Figure 2. 4	Distribution of sea level and surface current pattern on January and August	9
Figure 2. 5	Spatial distribution of the mean monthly highest tidal range in Indonesian Seas	10
Figure 2. 6	Mean monthly of wave height on January and August. Wave data is taken from altimeter Significant Wave Height (SWH) from January 2006 to December 2008	11
Figure 2. 7	The spreading pattern of chlorophyll-a on January and August	13
Figure 3. 1	Example of time-series of Sea Level Data from several stations in Indonesia and surrounding area.	17
Figure 3. 2	Flowchart of sea level rise estimation using historical data and IPCC model, that consist of 4 models, which are MRI, CCCMA CGCM 3.2, Miroc 3.2 and NASA GISS ER	18
Figure 3. 3	Climatology of sea level based on tide data, altimeter and model	19
Figure 3. 4	Morlet Wavelet	19
Figure 3. 5	Determination process of Nino3 that is used to estimate the occurrence of El Niño and La Niña	20
Figure 3. 6	Wavelet analysis result using Nino3 SST data and results for MRI model for SRESa1b scenario	21
Figure 3. 7	Height of tidal and direction of tidal current at 07.00 WIT before the lowest tide	21
Figure 3. 8	Speed and direction of tidal current at 07.00 WIT when head to the lowest tide	22
Figure 3. 9	Tide prediction based on 8 main harmonic constants using OTIS model and tide gauge data in Tanjung Priuk in Jakarta	22

Figure 4. 1	Time-series of SST based on paleoclimate data from 150 thousand years ago to 2005, with the highest SST occurring 125 thousand years ago, 30ºC in West Pacific and Indian Ocean, and 28 ºC in East Pacific (Hansen, 2006)	24
Figure 4. 2	The trend of SST rise based on the data of NOAA OI, with the highest increase trend occurring in Pacific Ocean in north of Papua, and the lowest in south coast of Java.	25
Figure 4. 3	The global trend of SST based upon observation data from 1870 to 2000, with the rate of SST rise reaching 0.4°C/century±0.17°C/century (Rayner, et al., 2003)	26
Figure 4. 4	The rate of SST rise based on IPCC SRESa1b, using MRI_CGCM 3.2 model	27
Figure 4. 5	Average sea level rise for 15 years from January 1993 to December 2008, using 0 cm as the lowest regional sea level	28
Figure 4. 6	The average magnitude of sea level from 2001 to 2008 subtracted from the average magnitude of sea level rise from 1993 to 2000, with the varying increase of sea level between 2 cm and 12 cm, and the average increase of 6 cm, in 7 years.	29
Figure 4. 7	The trend of sea level increase based on altimeter data from January 1993 to December 2008 using spatial trend analysis	30
Figure 4. 8	Approximation of sea level rise using a number of tidal data acquired from University of Hawai'i Sea Level Center (UHSLC)	31
Figure 4. 9	Approximation of global sea level change based on IPCC SRESa1b assuming the CO2 concentration is 750ppm	31
Figure 4. 10	Approximation of the amount of sea level rise in Indonesian waters based on scenario of IPCC SRESa1b, assuming the CO2 concentration is 750ppm	32
Figure 4. 11	Positive feedback of ice melting and the rising of surface temperature (UNEP/ GRID-ARENDAL, 2007)	34
Figure 4. 12	The change in Antarctica's temperature in the last 30 years	35
Figure 4. 13	The change of the ice-covering layer on Greenland based on analysis using satellite IceSAT (source: Earthobservatory, NASA, 2007)	36
Figure 4. 14	The sea level rise until year 2100, relative to sea level in 2000	36
Figure 4. 15	Estimated rate of sea level rise in Indonesian waters, based on model projections plus dynamic ice melting, post IPCC AR4	37

Figure 5. 1	An illustration of the scheme and causes of marine transportation accidents in the last few decades. SSH and SST indicates the sea surface height and sea surface temperature respectively.	40
Figure 5. 2	Sea level climatology based on tide gauge, altimeter, and IPCC model data. Model data were only displayed by sea level at the southern coast of Lombok Island.	41
Figure 5. 3	Result of wavelet analysis for historic data from 1871 to 1998. The dC indicates the degree Celsius	42
Figure 5. 4	Wavelet analysis results for the SRESa1b scenario. The dC indicates the degree Celsius	43
Figure 5. 5	Wavelet analysis results for the SRESa2 scenario. The dC indicates the degree Celsius	44
Figure 5. 6	Wavelet analysis results for the SRESb1scenario. The dC indicates the degree Celsius	44
Figure 5. 7	Time series of altimeter sea level anomaly from 1993 to 2008. Sea level anomaly falls to 20cm during strong El Niño, and rise 20cm during strong La Niña	46
Figure 5. 8	Hovmoller diagram of time-latitude sea level anomaly from 1993 to 2008, with lowest sea level anomaly in 1997/1998 during strong El Niño and the highest in 2008 during La Niña	46
Figure 5. 9	Average of significant wave height processed from altimeter from 2006 to 2008	47
Figure 5. 10	Hovmoller Diagram of daily time-latitude Significant Wave Height (SWH) with the lowest SWH happening in the area at 8°S to 4°N, also SWH height is inversely proportional between SWH in the South China Sea, Pacific and Sulawesi Sea (between 4°N to 12°N) with SWH in the Indian Ocean (between 8°S to 12°S)	48
Figure 5. 11	Maximum significant wave height during extreme wave, processed from the altimeter data of significant wave height from 2006 to 2008	49
Figure 5. 12	Time-series of wave height from January 1st 2006 to March 1st 2009 in Java Sea	49
Figure 5. 13	Time-series of wave height from January 1st 2006 to March 1st 2009 in the southern of Java Island	50

Figure 5. 14	Wind speed and direction on December 29th 2009	51
Figure 5. 15	SST anomaly from 90°E to 150°E and from 15°S to 15°N on August and September year 1980 to 2008. The increase of SST of more than 0.35°C shows strong La Niña period, and decrease of 0.35°C shows strong El Niño	52
Figure 5. 16	Chlorophyll-a distribution on September during normal condition, El Niño and La Niña	53
Figure 5. 17	Estimated locations where massive coral bleaching happens based on the difference of the highest sea level temperature to mean sea level temperature	54
Figure 5. 18	Coral bleaching sites as a result from SST increase in 1998 until 2006 (Marshall and Schuttenberg, 2006)	55
Figure 5. 19	Map of coral reef damage and coral bleaching based on data from Basereef. org	56
Figure 6. 1	Flow chart of process and general method for estimating sea-water-inundated area in year 2100	58
Figure 6. 2	Estimation of sea-water-inundated area due to influence of sea level rise which reach 1m, subsidence level of 3m per century, and 80cm of tide.	59
Figure 6. 3	Estimation of sea water-inundated area due to influence of sea level rise that reaches 1m, subsidence level of 2m per century, and 50cm of tide.	60
Figure 6. 4	Estimation of sea water-inundated area due to the influence of sea level rise that reaches 1m, subsidence level of 2.5 m per century, with highest tide as high as 1.5 m from MSL.	61
Figure 6. 5	Inundated area in Jakarta in year 2100 during extreme weather	62
Figure 6. 6	Inundated area in Semarang in year 2100 during extreme weather	62
Figure 6. 7	Inundated area in Surabaya in year 2100 during extreme weather	63

LIST OF ABBREVIATIONS

CGCM	Coupled General Circulation Model
ENSO	El Niño Southern Oscillation
GCM	General Circulation Model
GISS	Goddard Institute for Space Studies
GHG	Green House Gases
HYCOM	HYbrid Coordinate Ocean Model
IOSEC	Indian Ocean South Equatorial Current
IPCC	Intergovernmental Panel on Climate Change
ITF	Indonesian Through Flow
MODIS	Moderate Resolution Imaging Spectroradiometer
MRI	Meteorological Research Institute
NASA	National Aeronautics and Space Administration
NOAA	National Oceanic and Atmospheric Agency
OI	Optimum Interpolation
OTIS	Ocean Tidal Inverse Solution
PECC	Pacific Equatorial Counter Current
PNEC	Pacific North Equatorial Current
PSEC	Pacific South Equatorial Current
PTW	Pacific Trade Wind
SST	Sea Surface temperature
SRES	Special Report on Emission Scenario
SRTM	Shuttle Radar Topographic Mission
SWH	Significant Wave Height
TRMM	Total Rainfall Measurements Mission
UHSLC	University of Hawai'i Sea Level Center

1

INTRODUCTION

1.1 Background

It has been estimated that 23% of the world's population lives within both 100 km distance from the coast and less than 100 m elevation above sea level, and population densities in coastal regions are about three times higher than the global average (Small and Nicholls, 2003). This causes a serious vulnerability to the sea level rise caused by global warming. Meanwhile, human activities, in general, are believed to be the biggest contributors to the atmospheric built of greenhouse gases (GHGs), including water vapor (H_2O), carbon dioxide (CO_2), methane (CH_4), and chlorofluorocarbons (CFCs).

As the global warming process intensifies, the frequency of occurrence and intensity of El Niño and La Niña also increases (Timmerman et al, 1999). In general, El Niño occurs once in 2-7 years, but since 1970, the El Niño and La Niña frequency changes to once in 2-4 years (Torrence and Compo, 1999). Moreover, during El Niño in 1997/1998, Indonesia as a whole experienced a long dry season and during La Niña in 1999, Indonesia experienced a high increase of rainfall, with sea level rise ranging from 20 cm up to 30 cm. This combination of events led to floods in large areas of Indonesia, especially in the coastal region. Using sea level data on Java Sea from IPCC models, Sofian (2007) Predicted that the frequency of El Niño and La Niña events will become biennial during the period from year 2000 to 2100.

Aside from extreme climate events (e.g., El Niño and La Niña), global warming also causes sea level rise, both from the expansion of seawater volume as the result of temperature rise in the ocean and from the melting of glaciers and polar ice caps in the North and South Pole. Although the impact of sea level rise is only a subject of discussion among scientists, various climate change studies show that the sea level rise potential could range from 60 cm up to 100 cm, in year 2100. Regardless as the debate people living in the coastal area of Indonesia must have a broad awareness of the decrease of life quality in coastal regions due to sea level rise.

Globally, sea level rise (SLR) is about 3.1mm/year today, while the average sea level rise in the 20th century is only 1.7 mm/year. More than a third of sea level rise is caused by the melting of icecaps in the Greenland and the Antarctica, and by the retreat of glacial ice. Some recent research shows that the melting of glacial and polar ice will increase as global warming intensifies. If the warming and the melting of ice continue at a rate similar to that of the past 5 years, then the predicted sea level rise in 2100 could be as much as 80 cm to 180 cm.

The impacts and the consequences of SLR in various coastal regions will be influenced by numerous factors that interact with one another. These include up-thrusting of the land surface, subsidence, and coastal plantation conservation as a protection against inundation caused by SLR. Sea Level Rise has the potential to impact the people living in coastal environments of Indonesia, particularly along the northern coast of Java island, which is inhabited by more than 40 % of the country's total population. This risk creates an urgent need for action on adaptation (as well as mitigation) in order to assist the people who will face the consequences caused by sea level rise. It is hoped that this study will provide the basic for the concrete guidance on how best to adapt to the impact and consequences of sea level rise in shoreline and

coastal environments. One approach to understanding the correlations among climate change, adaptation study, and the planning of prudent response strategies are illustrated in Figure 1.1.

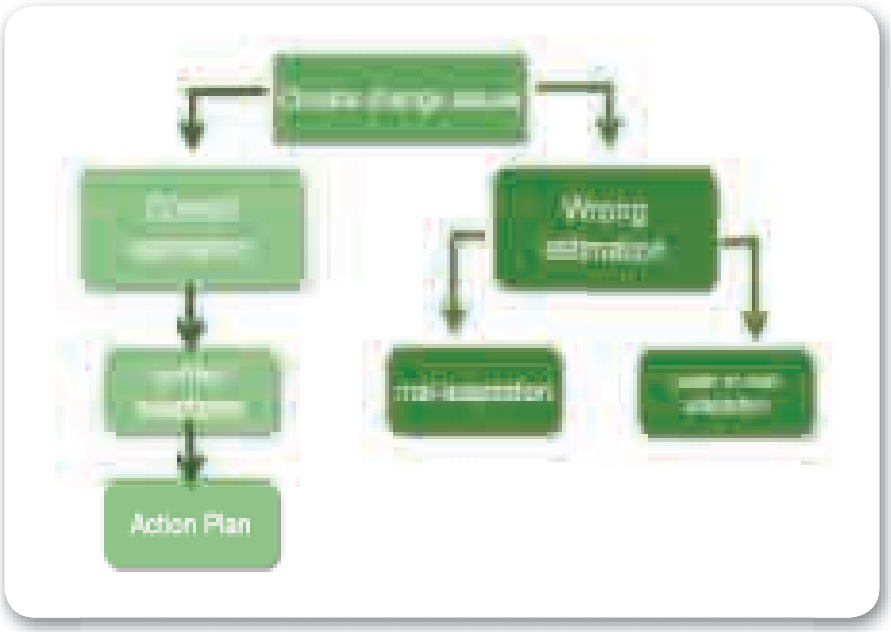

Figure 1. 1 Flow chart of climate change study to support for climate change adaptation action plan

1.2 Aims and Objectives

The aims of this study are as follows:

1. To investigate the SLR rate caused by the global warming.
2. To investigate the impacts of global warming on the sea surface temperature (SST), the intensity of extreme events and their impacts on the significant wave height characteristics.

Meanwhile, the purposes of this study are:

1. To provide a base reference and information for resilient coastal area development, in order to adapt to the risks of future climate change, particularly sea level rise (SLR).
2. In addition, by identifying the base reference, adaptation plan for reducing the risks of sea level rise could be well prepared.

Aside from sea level rise projection, this study will analyze the changing frequency and severity of extreme events caused by global warming and, in particular, of the effects of global warming to La Niña and El Niño, which are also referred to as ENSO (El Niño Southern Oscillation). The time-frequency

analysis for extreme events was conducted using wavelet analysis to find the moment and frequency of occurrences of El Niño and La Niña.

This study is structured as follows: the first chapter contains an introduction that includes the background and objectives of the study; the second chapter outlines the climate and oceanographic condition of Indonesian Seas. It covers sea level and surface temperature climatology, chlorophyll-a spatial distribution, and wave height. The third chapter explains the methodology and the data used for our analysis, while the fourth chapter presents the projection of sea surface temperature (SST) and sea level. It is followed by the fifth chapter on ENSO projection, based on sea surface temperature in the Nino3 area (defined as area between 5°S and 5°N and between 210°E and 270°E), and the analysis of ENSO effects on the characteristics of sea level, chlorophyll-a spatial distribution, SST, and wave height. The last chapter contains our conclusions and recommendations for adaptation to the risks of disaster due to sea level rise caused by global warming and ENSO.

2

CLIMATE AND OCEANOGRAPHIC CONDITION IN INDONESIAN SEAS

Indonesia is a maritime country located between two oceans, the Indonesian Ocean and the Pacific Ocean. This unique geophysical position affects the monsoon pattern, rainfall, and other characteristics of regional climate.

2.1 Wind and Rain Patterns

In the northwesterly wind season from October to March (i.e., when wind blows from the west), the weather in Indonesia is affected by the northwest monsoon. During this period, the wind blows from the northeast and turns to the southeast after passing through the equator. By contrast, in the season of the southeasterly wind from May to September, the wind blows from southeast and turns to northeast after passing through the equator. The influence of the Pacific Ocean is dominant in the period of westerly wind (except in most part of Sumatera, which is affected by the western Indian Ocean). Meanwhile during the season of the easterly wind, the influence of the Indian Ocean is dominant, and is marked by reduced rainfall on Java Island and in Nusa Tenggara. However, during this period, most parts of Sumatera and Kalimantan still have high probability of experiencing medium intensity of rainfall.

The propagation of northerly wind from October to March pushes down the warm seawater from the Pacific Ocean to the Indian Ocean. This causes high rainfall in almost every area of Indonesia. While in the season of easterly wind from May to September, eastern wind pressure pushes the low temperature seawater back from the Indian Ocean to the Pacific Ocean through the Java Sea, the Karimata Strait and the South China Sea. This period is marked by decreasing rainfall in Java, Kalimantan and southern Sumatera. At the same time, in the Riau Islands, western Sumatera may still have rain due to the high SST around those areas.

Figure 2.1 shows the wind pattern and spatial distribution of SST in January during the peak of west wind season and in August during the peak of the east wind season. The wind pattern and SST are taken from the Quick Scat (Quick Scatterometer) and NOAA (National Oceanic and Atmospheric Agency) OI (Optimal Interpolation) respectively. The monthly rainfall for January and August are based on the data of TRMM (Total Rainfall Measurements Mission) that can be seen in Figure 2.2. From Figures 2.1 and 2.2, the strong relation between rainfall pattern and SST distribution can be seen. In January, high rainfall levels (i.e., between approximately 250 mm and 400mm are visible in almost every area of Indonesia, which is, accompanied by high SST (i.e., above 28°C). In August, the low rate of total rainfall in Indonesia (i.e., below 50mm/month), is visible, especially in the area of southern equator, and SST is generally below 27°C.

a. January

b. August

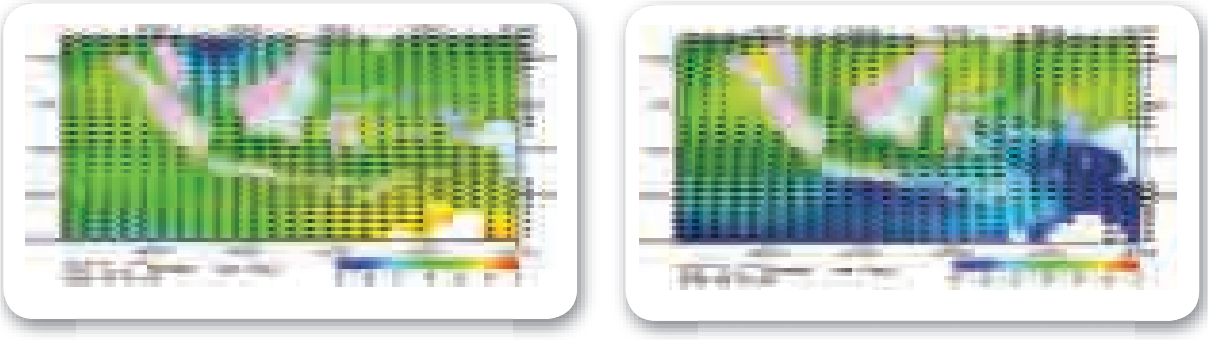

Figure 2. 1 The pattern of wind and sea level temperature (SLT) in January and August

a. January

b. August

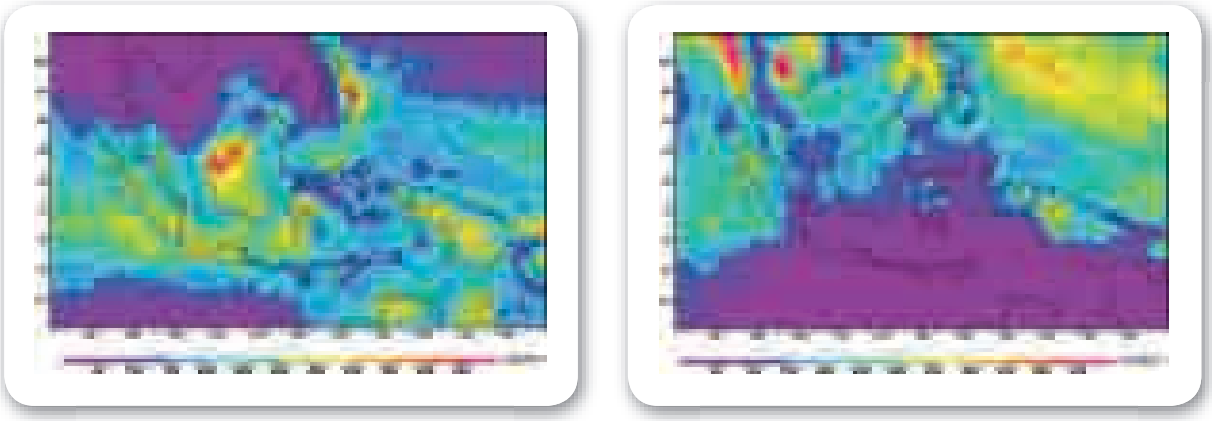

Figure 2. 2 Annual cycle of mean rainfall in Indonesia in January and August

2.2 Sea Level Variations

2.2.1 Ocean Currents and Sea Level

Generally, the pattern of Indonesian Through Flow (ITF) affects the climate characteristics of the region through the heat-transfer mechanism between Pacific Ocean and Indonesian Seas. Figure 2.3 shows surface flow and spatial distribution of sea level on January and August. Flow pattern and sea level estimation have been calculated using HYbrid Coordinate Ocean Model (HYCOM, Bleck 2002). The model configuration for Java Sea, Makassar Strait and some part of South China Sea can be seen in Sofian, 2007.

a. January

b. August

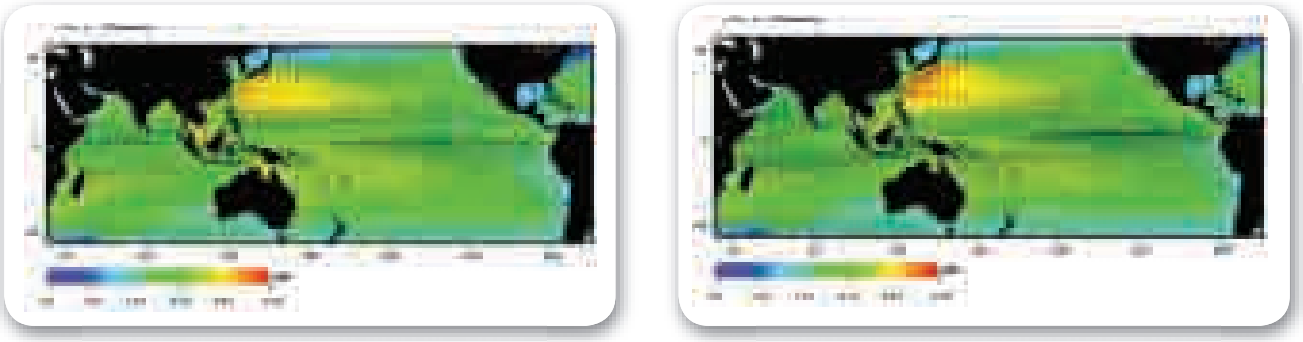

Figure 2. 3 Spatial distribution of SLH and surface current in January and August. SLH is based on altimeter data, while the direction and the speed of current is an estimation result using HYCOM (HYbrid Coordinate Ocean Model) (Sofian, 2007)

In general, sea level in Indonesian waters is high in January (northwest monsoon) and low in August (southeast monsoon). Meanwhile the yellow lines and arrows in Figure 2.3 illustrate the surface flows of the Indian Ocean South Equatorial Current (IOSEC). Each of the white and solid red line and arrow illustrate the Indonesian Through Flow (ITF) from the South Pacific to Indian Ocean, through the Makassar and Lombok straits, and also the South China Sea, Karimata Strait, and Java Sea. The red dotted line and arrow indicate the surface flows of the Pacific South Equatorial Current (PSEC), with SEC and ITF sketches based on Vranes et al. (2003). In the period of west monsoon, i.e., January, Figure 2.3 (a.) illustrates that the IOSEC move westward in the region of 10°S to 20°S, while mesoscale eddies are not clearly seen in the South China Sea. The strong surface current in the South China Sea causes the increasing sea level from western and northern Kalimantan to eastern Vietnam. Then the PSEC located between latitude 5°N to 15°S until 20°S flows westward due to the blowing of the Pacific Trade Wind (PTW) from the aquatic zone around Peru to longitude 180°E. Meanwhile, the Pacific North Equatorial Current (PNEC), which is normally located between latitude 10° to 25° N, is heading westward by the southeasterly trade wind. When PNEC reaches the Philippines, this surface current is broken, with the smaller part moving to the south to form the Pacific Equatorial Counter Current (PECC), while the biggest part moves to the north to form the Kuroshiyo current. In addition, the current in Makassar Strait weakens due to the strength of the surface current of the Java Sea.

Figure 2.3 (b) shows sea level and current vector in August during the southeast monsoon. Eastward-moving surface current in South China Sea pushes down seawater to the east and produces high sea level from northwestern coasts of Kalimantan to the northeastern Philippines. Meanwhile, IOSEC's expansion moves northward from latitude 16°S during west monsoon to latitude 8°S. The PSEC surface current is stronger compared to the one in northwest monsoon. The PNEC is weakening and Kuroshiyo current is dominated by the strong surface current from the South China Sea that moves to the north. In addition, the southward Makassar Strait surface current is getting stronger and heading to the Indian

Ocean through the Lombok Strait.

Figure 2.4 shows the pattern of monthly average surface current and sea level over a period of 7 years from 1993 to 1999, measured in January and August. Current pattern and sea level height estimation based on the HYbrid Coordinate Ocean Model (HYCOM, Bleck 2002). Model configuration for the Java Sea, Makassar Strait and most parts of the South China Sea is outlined in Sofian et al, (2008).

a. January

b. August

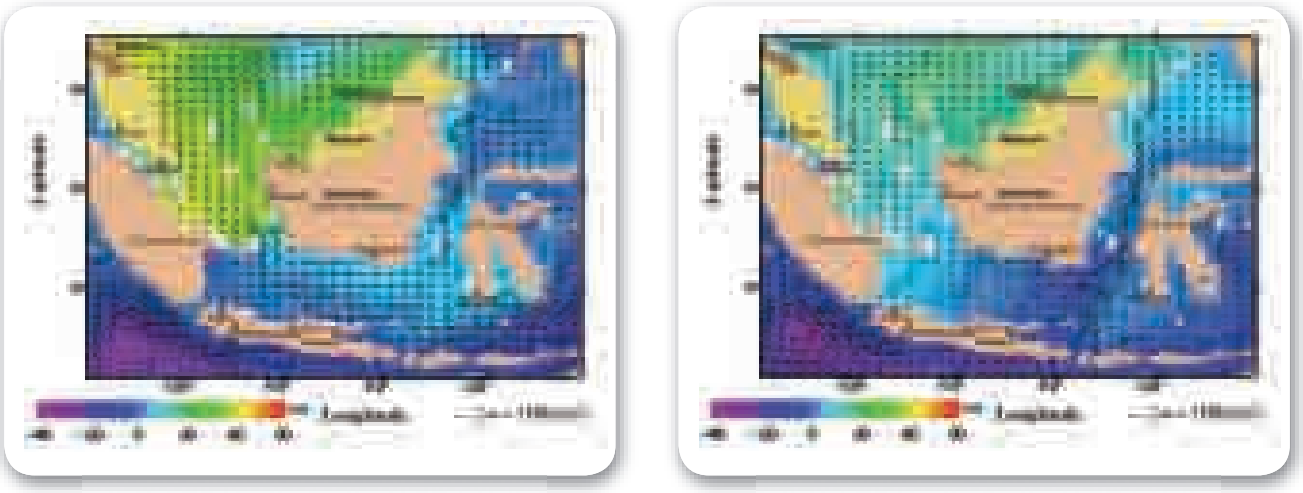

Figure 2. 4 Distribution of sea level and surface current pattern in January and August. The sea level and the current pattern are the monthly average in 7 years, from 1993 to 1999

Figure 2.4 (a) shows the current patterns in January during the southwest monsoon. The propagation of southwesterly wind causes the current in the Java Sea to flow eastward and the water from the Indian Ocean enters into the Java Sea via the Sunda Strait. The topographic effect of the shrinking and shallowing of the southern Karimata Strait's depth, causes a 40 cm of sea level difference between the Java Sea and the Karimata Strait. Moreover, the current pressure to the east causes the gradient of sea level height difference, with a decreasing of sea level height in the Java Sea and an increase of the sea level in Banda Sea, as well as along the northern coast of Lombok Island (as can be seen for January in Figure 2.4). These wind patterns change as the seasons change. The wind that blows from southeast in the dry season (i.e., during the southeast monsoon) pushes the current in the Java sea to the west, while the current in Karimata strait moves to the north (Figure 2.4). The Java Sea surface water then flows out through Sunda Strait as seen in Figure 2.4.

The pattern of surface currents in the Makassar Strait differs from current pattern in the Java Sea and the Karimata Strait and does not follow the pattern and direction of seasonal winds. The Makassar Strait surface current tends to move southward. The speed of the surface current in the Makassar Strait is weak during the northwest monsoon, although the northerly wind is very intensive. It is caused by the strong surface current in the Java Sea that inhibits the southward Makassar Strait surface flow. Moreover, the

surface current in the Makassar Strait strengthens in the dry season (with the southeasterly wind), and pushes the low salinity and temperature surface water back to the Java Sea. The strong Makassar Strait surface flow also causes the decreasing of sea level along the northern coasts of Lombok Island, Flores Sea, eastern and middle Java Sea on August, as seen in Figure 2.4 b).

2.2.2 Tidal Forcing

The OTIS model is calculated based on assimilation between the tide gauge and altimeter data from October 1992 to December 2008. Moreover, the average of the highest tidal range is depicted in Figure 2.5.

Based on OTIS model for Indonesia, it is known that the highest tidal range occurs in the southern coast of Papua Island that reaches 5 m, with each highest and lowest tide is about 2.6 m to -2.6m. The Southern Karimata Strait has the tidal range between 2.2m and 2.4m, with highest tide reaches 1.2m, and lowest tide between -1.1 m and 1.1 m. The tidal range height in Java Sea is about between 1.2 m and 2m, with the highest tidal range in the eastern Java Sea around Surabaya, Madura, and Bali. It is also seen that there is a time difference of the highest tide occurring in the Java Sea, with the highest tide is in around Jakarta, occurring in 00.00 WIT until 01.00 WIT, and then shifted to the east, with the highest tide is around Bali in 12.00 WIT (figure not shown).

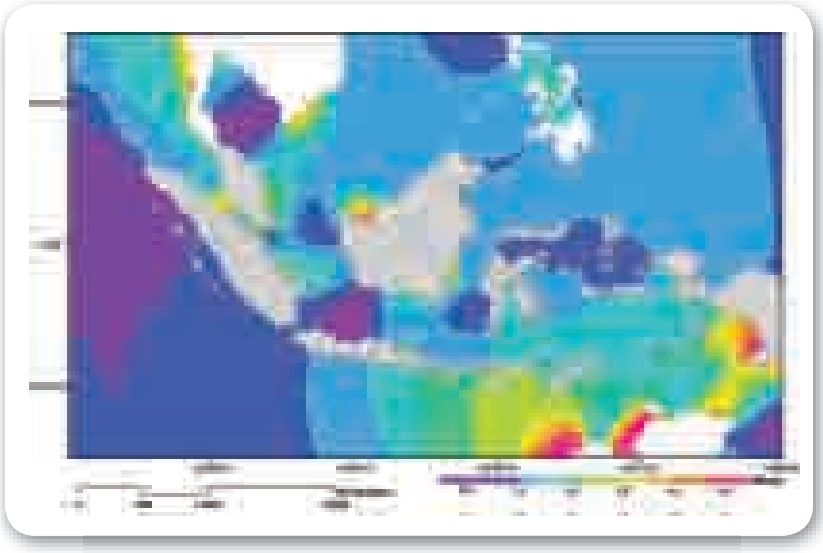

Figure 2. 5 Spatial distribution of the monthly mean highest tidal range in the Indonesian Seas

Meanwhile the tidal occurring in the west coast of Kalimantan Island has the highest tide of 2m and the lowest tide is about -2m, each occurs at 06.00 WIT and 00.00 WIT. The height of the tide in the South Sulawesi is about 1.2m to 1.4m, and reaches 1.6m to 1.8 m in the North Sulawesi, the lowest tide reaches -1.4m and -1.8m respectively.

2.2.3 Significant Wave Height

Figure 2.6 illustrates a 3-year average of wave height data for January and August that was obtained from altimeter data of Significant Wave Height (SWH). The average wave height in January ranges from about 60cm to 240cm, with the highest waves reaching 3m and occurring in the West Pacific, in north of Papua. The wave height characteristic over the north of equator has the highest annual wave during January, except along the west coast of Sumatera where it is bordered by the Indian Ocean.

a. January

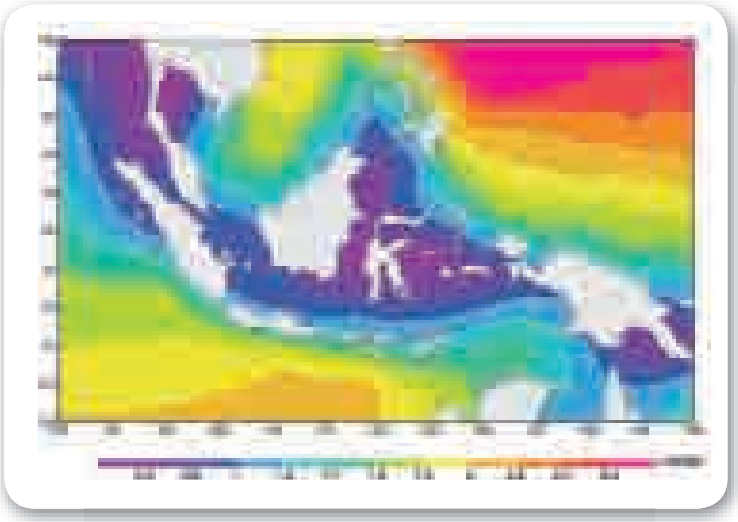

b. August

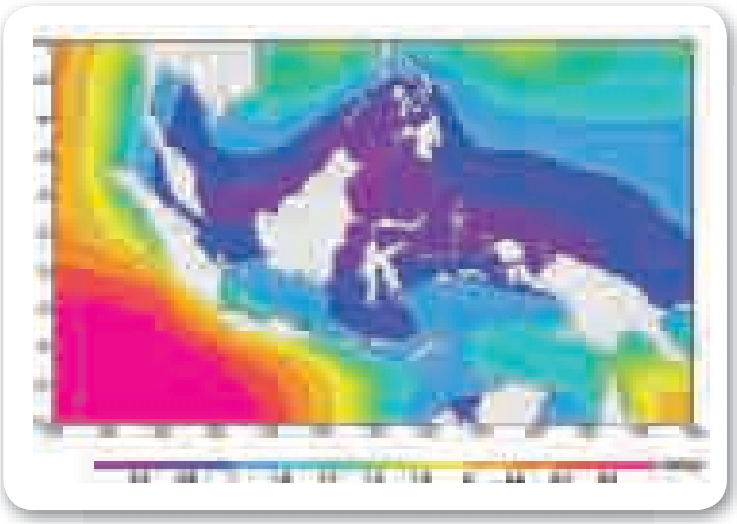

Figure 2. 6 Mean monthly of wave height in January and August. Wave data is taken from altimeter *Significant Wave Height* (SWH) from January 2006 to December 2008

In contrast, the area that is located south of the Equator has the highest annual waves in July and August. In addition, the highest waves in August occur in the Indian Ocean, with the height exceeding 3m, whereas the wave height in the Makassar Strait, the Karimata Strait, and the aquatic around Ambon island, have the lowest wave height, with a range of about 60 cm to 1 m. In addition, the wave height in Java Sea reaches its highest point in July to August, with a range of about 1.2 m to 1.4 m.

2.3 The Distribution of Chlorophyll-a and Sea Surface Temperature

Along with the seasonal wind pattern, the spatial distribution of chlorophyll-a in January and August is shown in Figure 2.7, based on the Seawifs data. Generally, the chlorophyll-a concentration is low in January in northwest monsoon, although medium and high concentration of chlorophyll-a is still seen in West Kalimantan, Riau Islands and Java Sea. However, it shows high turbidity level due to the wind propagation that causes the perfect mixing layer formation to the bottom. This is because of the Java Sea, Riau Island and South Karimata Strait have average depth less than 50m.

a. January

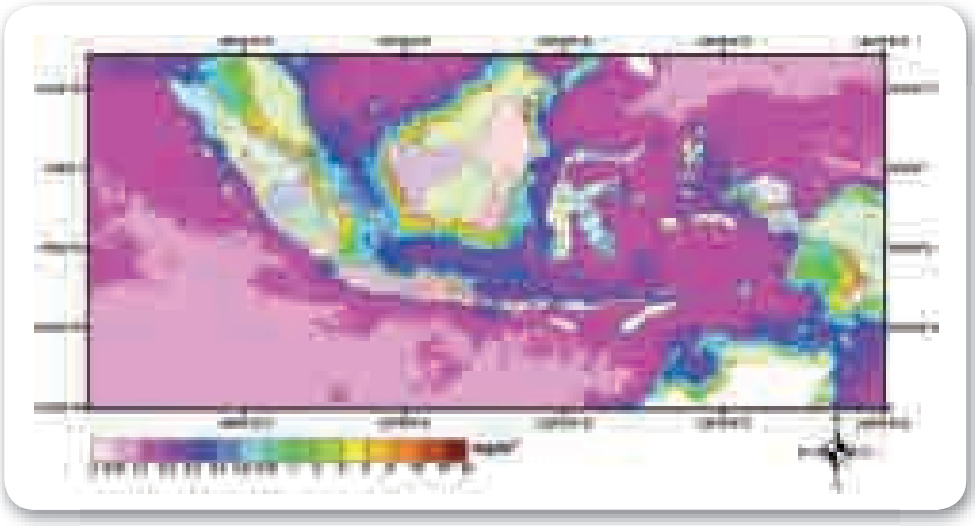

b. August

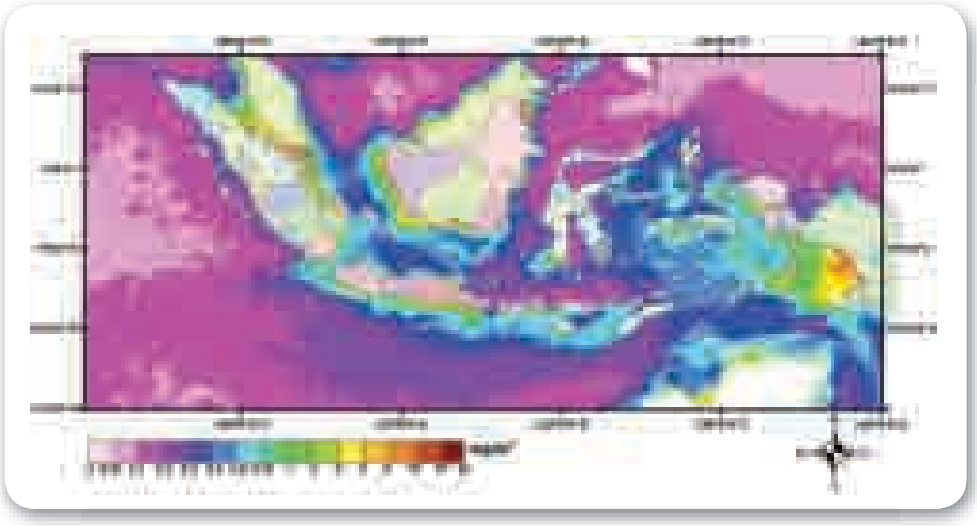

Figure 2. 7 The spreading pattern of chlorophyll-a in January and August

The chlorophyll-a concentration in the deep ocean such as the Indian Ocean of south Java Island is decreasing because of the down-welling due to the propagation of westerly wind. SST increases due to the warm water of sea level from the Pacific Ocean (Figure 2.1). This causes a decrease in fishing potential. Meanwhile, in August it increases especially in Indian Ocean, because the upwelling process is getting intensive due to the strong easterly wind. The concentration of chlorophyll-a is concentrated in the Indian Ocean south of Java Island with a concentration of more than 3mg/m3. Moreover, the fishing potentials in the Java Sea and the Riau Islands water are also increasing, due to the transfer of colder seawater from the Indian Ocean, through the Banda Sea.

3

METHODOLOGY

3.1 Data

Sea level data used in this study includes:

1. Historical data consisting of:

   - Tidal data which was compiled from the following stations: Surabaya, Benoa, Darwin, Broome, Ambon, Singapore, Jakarta, Bitung, Sibolga, Manila and Sandakan. Monthly sea level average is defined as sea level during that month minus average sea level for the period of observation. All tidal data is obtained from the UHSLC (University of Hawaii Sea Level Center). Figure 3.1 shows time-series data for monthly sea level from several tide gauge stations.

   - Altimeter data from several satellites have been merged for this study. Altimeter satellites used for this study include TOPEX/Poseidon (T/P), GFO, Envisat, ERS-1 and 2, also Jason-1, that is provided since October 1992 to October 2008. The altimeter data for this study was obtained from AVISO (AVISO, 2004).

2. Model output data for the period of 2000 - 2100 was obtained from the IPCC Special Report on Emission Scenario (SRES), focusing on scenarios b1, a1b and b2. These scenarios project CO_2 concentration in 2100 of up to 750 ppm (part per million by volume) and 540 ppm. For this study, the primary emphasis has been placed on the analysis results using the Scenario a1b SRES. The IPCC data used for this analysis include the data for sea surface temperature and sea level, along with the output data from MRI_CGCM2.3 (Japan), CCCMA_CGCM3.2 (Canada), Miroc3.2 (Japan), and NASA GISS ER (USA) model.

3. Supporting data used in this study include:

   - Data on sea surface temperature derived from NOAA (National Oceanic and Atmospheric Agency) OI (Optimal Interpolation) (Reynolds, 1994) for the period of 1981 until 2008.

   - Estimation of chlorophyll-a concentration data using MODIS and SeaWifs data.

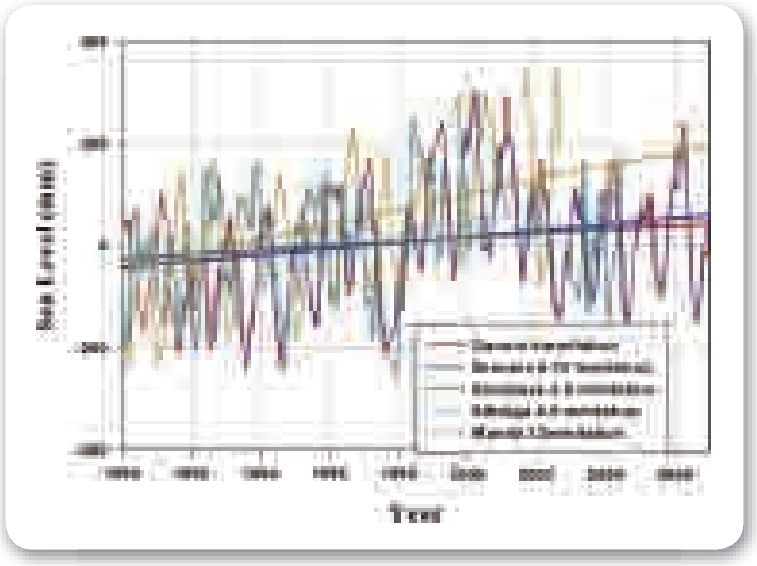

Figure 3. 1 Example of time-series of Sea Level Data from several stations in Indonesia and surrounding area.

3.2 Method

For this study, the method used to estimate sea level rise and the occurrence of extreme events (e.g., El Niño and La Niña), involve:

1. Trend analysis to expose the tendency and rate of sea level rise based on the historical data, including altimeter satellite data and tide data, along with the IPCC modeling output data. In this case, the trend analysis was developed as a linear regression of sea level by month, with the following mathematic equation of $y = a + bt$,

Where y is sea level, t is time stated in months,

a is offset, and b is the rise rate (slope, trend).

The detail of the sea level rise extrapolation by trend analysis is shown in Figure 3.2 below.

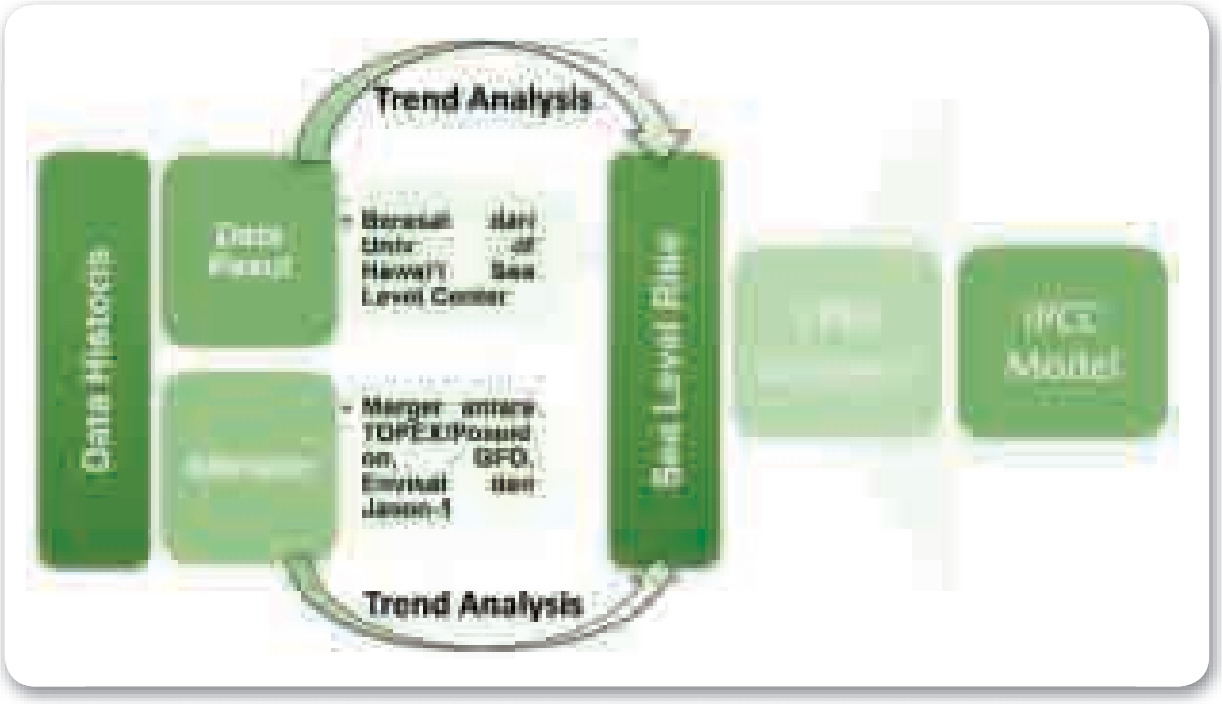

Figure 3. 2 Flowchart of sea level rise estimation using historical data and IPCC model, which consists of 4 models, which are MRI, CCCMA CGCM 3.2, Miroc 3.2 and NASA GISS ER

2. Composing climate data to figure out the effect of monsoon to the characteristic of chlorophyll-a, rainfall, SST, and sea level. The climate analysis result is also used to detect the consistency of model to historical data. Figure 3.3 shows a comparison of observed climate data from the waters of Lombok Island using sea level data with model results. Projections from the Meteorological Research Institute (MRI) model from Japan, which has the same character as tidal data and altimeter data, suggests that the lowest sea level is in August until September, and the highest sea levels is in January until April. Based on this comparation test, SST data from the MRI model is used as reference to detect the occurrences of extreme events that would be explained at point 3.

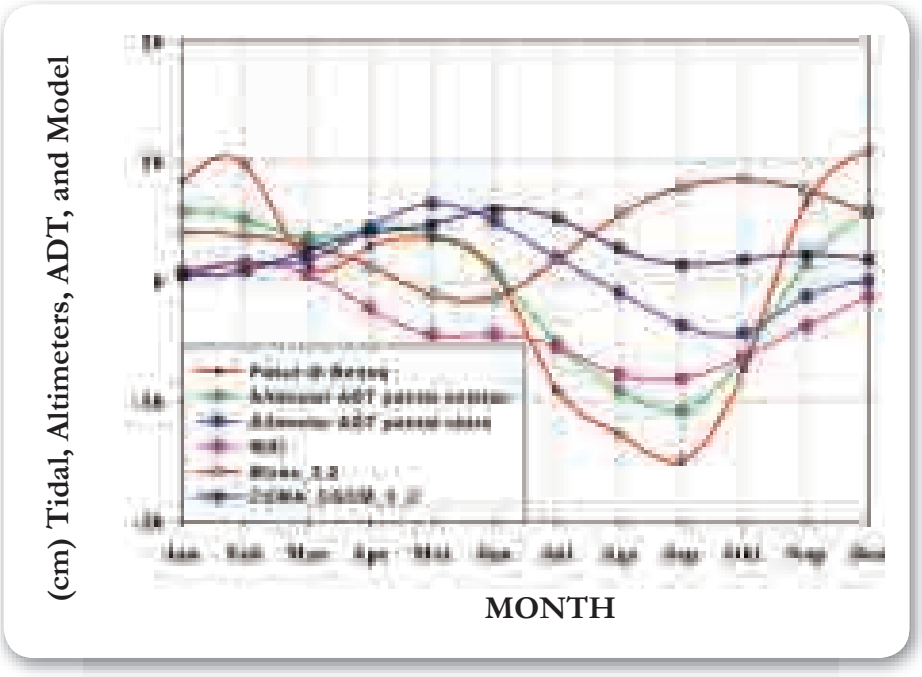

Figure 3. 3 Climatology of sea level based on tide data, altimeter and model

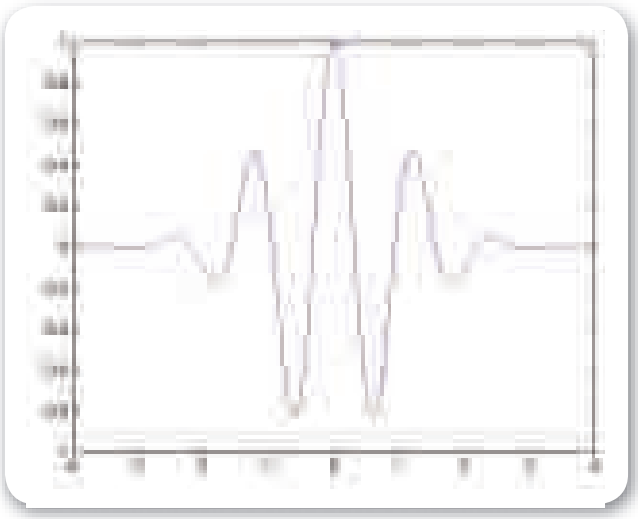

Figure 3. 4 Morlet Wavelet

3. Wavelet analysis is used to detect the time and occurrence of El Niño and La Niña from the year 2000 until 2100. The detailed description and numerical algorithm that is used in the wavelet analysis is taken from Torrence and Compo (1999). Wavelet analysis is also used as a method for conducting Time-frequency analysis. Wavelet model that is used to detect the time and the frequency of El Niño and La Niña (ENSO or El Niño Southern Oscillation) is the sixth order of Morlet function. Morlet function can be illustrated as shown in Figure 3.4. Wavelet transformation is used to detect

non-stationary phenomena (signal with changing frequency). The wavelet transformation approach has several advantages compared to the alternative Fourier transformation that is frequently used. By comparison, Fourier transformation can only be used to detect stationary phenomena (signal with constant frequency).

The time and frequency of ENSO occurrence can be determined by using wavelet analysis of SST in East Pacific. The SST is defined between 150°WL (west longitude) to 90°WL and from 5°NL (North Latitude) to 5°S (South Latitude), which is sometimes referred to as the Nino3 area. The application of this process to Nino3 area in order to create the ENSO index is shown in Figure 3.5. An example of applying the detection process to an extreme climate event is illustrated in Figure 3.6. Details of the explanation concerning extreme climate events are described in Chapter V.

2 The calculation of tidal forcing is done by using an OTIS (Ocean Tidal Inverse Solutions) that we acquired from the Oregon State University. The OTIS is based on the altimeter data for the year 1992 to 2008, primarily with emphasis to the TOPEX/Poseidon data. The OTIS calculation is built using a method of assimilation for both altimeter and tidal gauge data. The numerical algorithm and mathematical equation used in the OTIS model is shown in Egbert, et al. (1994). OTIS has several advantages compared to pure tidal gauge data. Most importantly, it can predict the current and height of tides in the open sea with high accuracy. An example of sea level calculations based on an OTIS model is shown in Figure 3.7. Meanwhile, the tidal data for the same period is illustrated in Figure 3.8. In addition, a validation test between the OTIS model run and tidal station data for Jakarta is shown in Figure 3.9. This analysis applies tidal prediction process using 8 main harmonic constants, namely O1, K1, M2, S2, N2, Q1, P1, and K2. Validation test result shows that the OTIS output has a correlation up to 0.7 with Root Mean Square Error (RMSE) up to 10 cm.

Figure 3. 5 Determination process of Nino3 used to estimate the occurrence of El Niño and La Niña

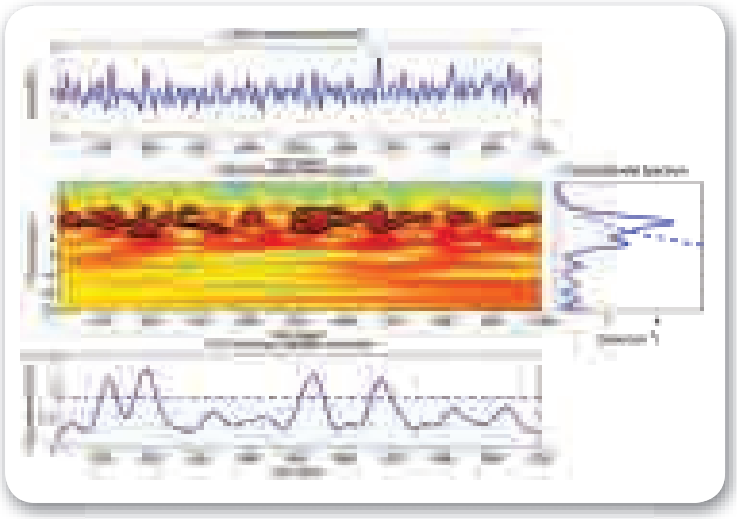

Figure 3. 6 Wavelet analysis result using Nino3 SST data and results from the MRI model for SRESa1b scenario

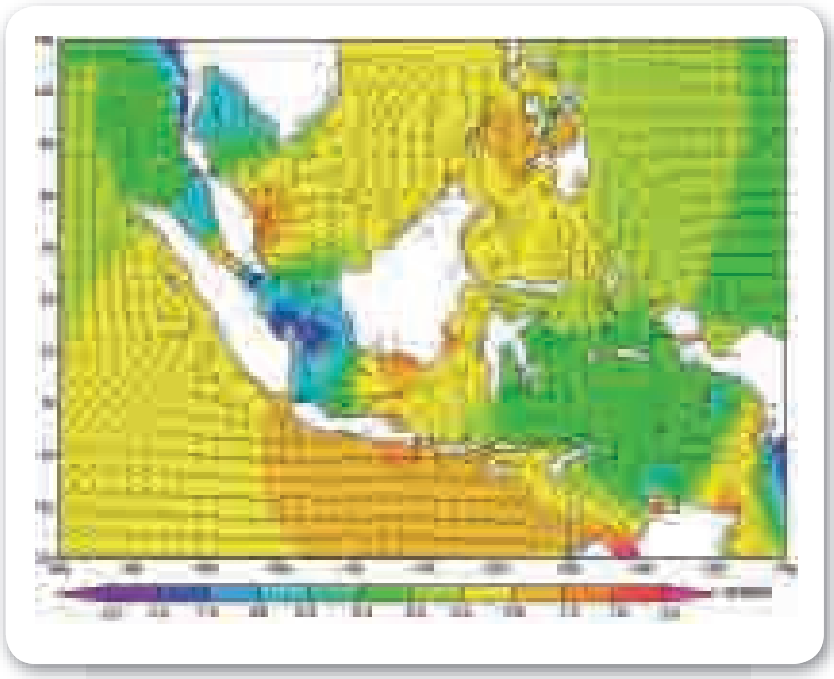

Figure 3. 7 Height and direction of tidal current at 07.00 WIT before the lowest tide

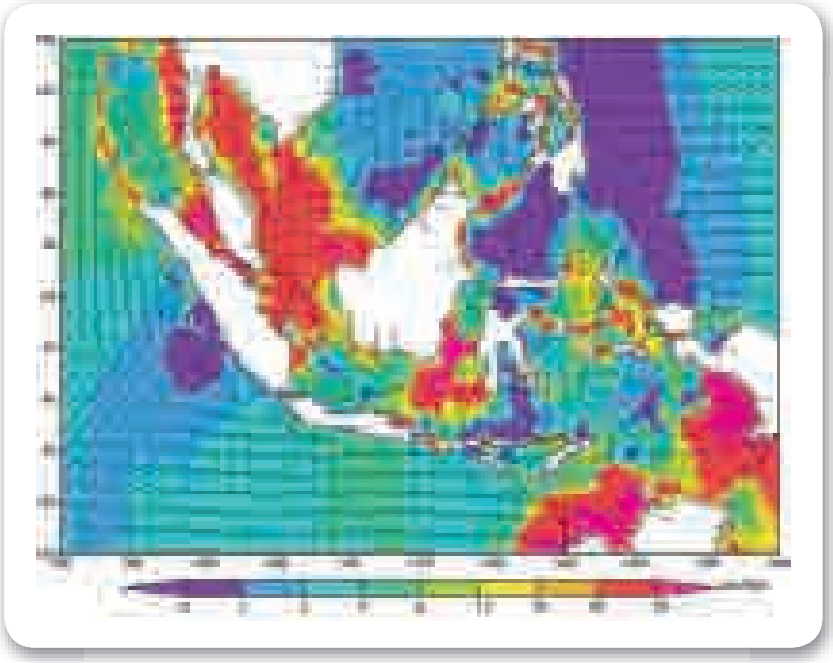

Figure 3. 8 Speed and direction of tidal current at 07.00 WIT when is heading to the lowest tide

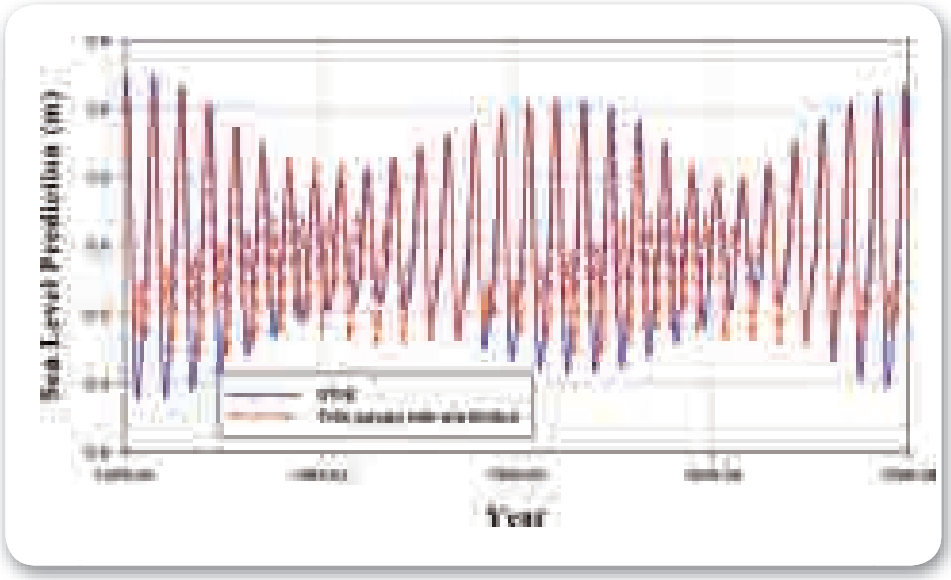

Figure 3. 9 Tide prediction based on 8 main harmonic constants using OTIS model and tide gauge data in Tanjung Priuk in Jakarta

4

PROJECTION OF SEA LEVEL RISE AND SEA SURFACE TEMPERATURE

Global warming resulted from the atmospheric buildup of greenhouse gases has an important effect on sea level. In general, the gradual increase of sea level caused by global warming is one of the most complicated aspects of the global warming effect, as its acceleration rate is a function of the intensification of global warming. Sea level rise is affected by the addition of water mass, which results from the melting of glaciers and ice sheet in the Greenland and the Antarctica, as well as from the increase in water volume due to thermal expansion of the upper mixed layer (with fixed water mass), which is caused by the rising water temperature. This chapter explains the projection of SST and sea level rise based on the NOAA OI SST, tidal and altimeter data, and model results from the IPCC portal.

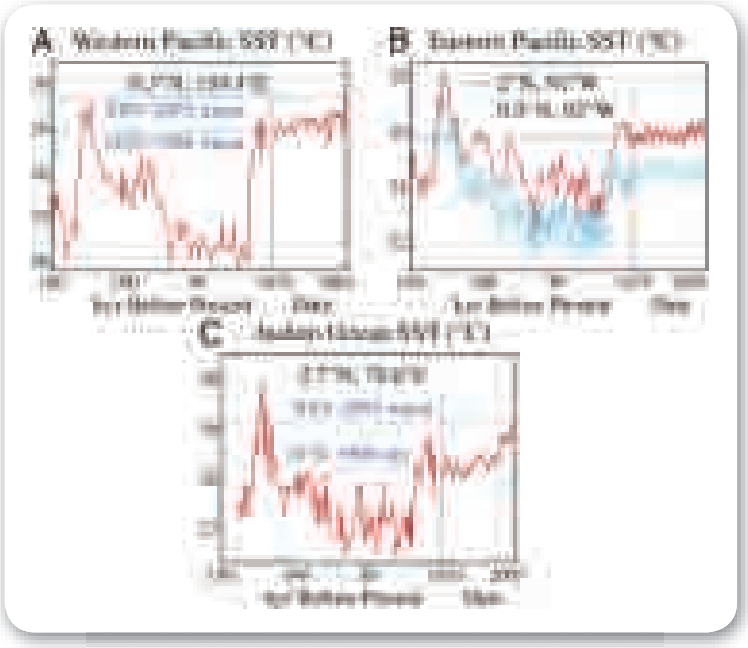

Figure 4. 1 Time-series of SST data based on paleoclimate data from 150 thousand years ago to 2005, with the highest SST occurring 125 thousand years ago, 30ºC in the West Pacific and the Indian Ocean, and 28 ºC in the East Pacific (Hansen, 2006)

4.1 Sea Surface Temperature Rise Projection

Based on the paleoclimate data of the Pacific and Indian Ocean (Figure 4.1, Hansen, 2006), it can be deduced that the highest sea surface temperature occurred 125 thousand years ago, when the sea reached 30ºC in the West Pacific and Indian Oceans, and 28 ºC in the East Pacific Ocean. From Figure 4.1, it can be seen that an abrupt change of SST has occurred during the last 10 thousand years, with 2ºC to 3ºC increase until 1870. Since 1870, sea surface temperature (SST) rise has accelerated due to GHG emissions associated with the industrial revolution in Europe and America. The acceleration rate of SST rise has continued to increase since the 1990s. If SST increases by 1ºC to 2ºC above the 2005 level, the SST will then exceed the highest sea surface temperature of the last 150 thousand years.

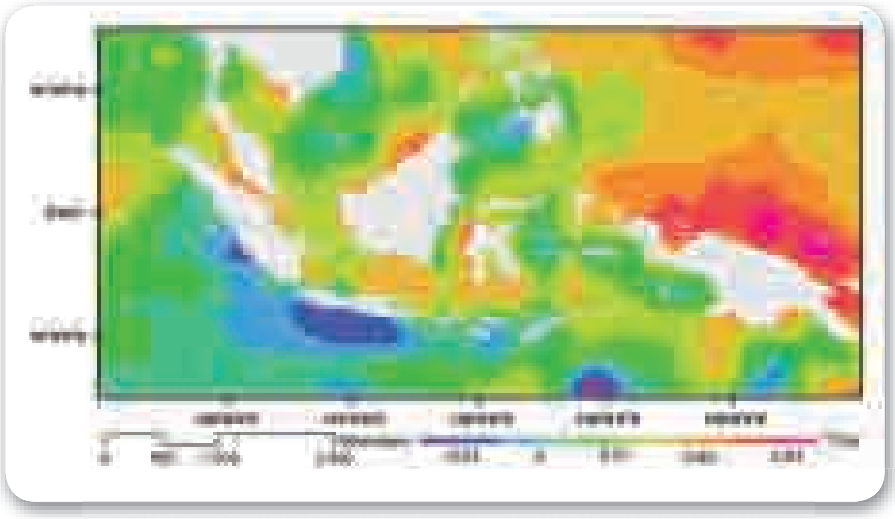

Figure 4. 2 The trend of SST rise based on the data of NOAA OI, with the highest increase trend occurring in the Pacific Ocean in the north of Papua, and the lowest in the south coast of Java.

The modern record of SST is based on the monthly SST data provided by the U.S. National Oceanographic and Atmospheric Agency (NOAA). The primary dataset is the Optimum Interpolation (OI) version 2 (Reynolds, 1994), from year 1983 to 2008, as shown in Figure 4.2. Figure 4.2 illustrates the variation of SST rise rate of -0.01°C/year to 0.04°C/year, where the highest trend occur off the northern coast of Papua Island, and the lowest one occur on the south of Java Island. However, this negative trend does not indicate the long-term SST changing rate within this area for the future. This negative rise rate could have been caused by the increasing frequency of El Nino and the elevated wind speed coming from the southern Indian Ocean, which will be explained in Chapter V.

For comparison, the average trend of the SST rise rate in the Indonesian waters ranges from 0.020°C/year to 0.023°C/year. Based on this, it can be concluded that the SST in year 2030 will reach 0.6°C to 0.7°C, and will reach 1°C to 1.2°C in year 2050, relative to the average SST in 2000. In addition to that, SST is expected to rise by 1.6°C to 1.8°C in year 2080, and could reach 2°C to 2.3°C in year 2100. This would indicate that the projected SST in 2050 is the highest temperature during the last 150 thousand years, when compared to SST detected in paleoclimatic data for the western Pacific Ocean.

Figure 4.3 shows the time-series of global SST, with the rise rate ranges from 0.3°C/century to 0.4°C/century, relative to 1870. The global SST rise rate is getting higher from time to time, with the rise rate reaching 0.7°C/century since 1910. Looking just at the period since 1970, the rise rate has sharply increase to approximately 1.4°C/century to 1.5°C/century. Based on the current trend of average global SST rise rate, by year 2130, the global SST will reach the highest level since 150 thousand years ago.

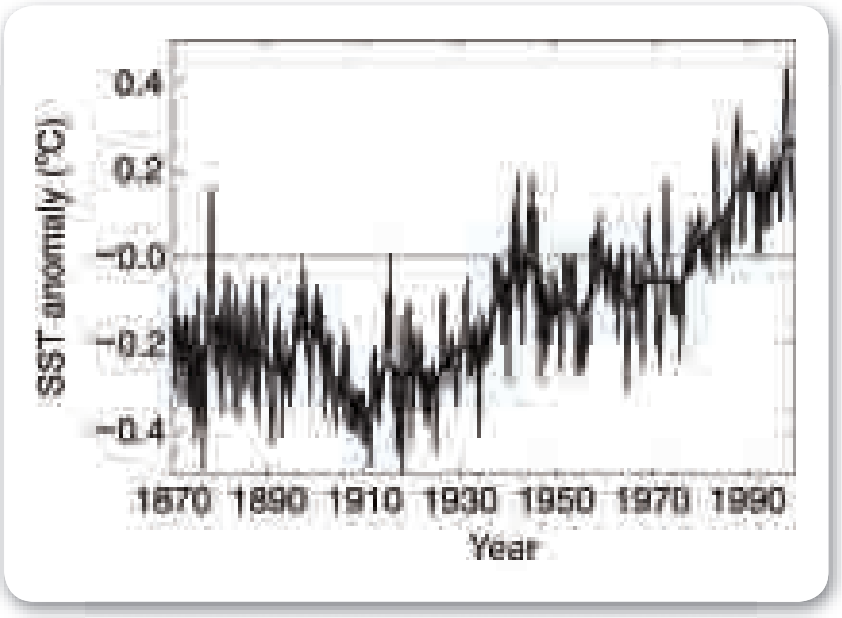

Figure 4. 3 The global trend of SST based upon observation data from 1870 to 2000, with the rate of SST rise reaching 0.4°C/century±0.17°C/century (Rayner, et al., 2003)

Based on the MRI CGCM SRES A1b, the spatial distribution of SST rise rate ranges from 0.014ºC/year to 0.030ºC/year. This pattern is depicted in Figure 4.4, with the average SST rise rate across Indonesia ranges from 0.021 ºC/year to 0.023 ºC/year. The results from model estimation is relatively matching to the observational data, even though the model-estimated SST tends to be higher, with small gap between the highest and the lowest trend (approximately 0.07 ºC/year). Nevertheless, compared to observation data, model estimation also indicates a greater spatial difference in the trend for the northern Indian Ocean, near India. Therefore, based on the model results, the trend of sea-surface temperature rise in 2030 will reach 0.6 ºC to 0.7ºC. At that rate, the rise of SST will reach 1.05ºC to 1.15ºC in 2050. In year 2080, the cumulative increase in sea-surface temperature will reach 1.7ºC to 1.8ºC, and ultimately 2.1ºC to 2.3ºC, relative to SST in 2000. The summary of sea-surface temperature rise, based on satellite data (observation) and model data, is shown in Table 4-1.

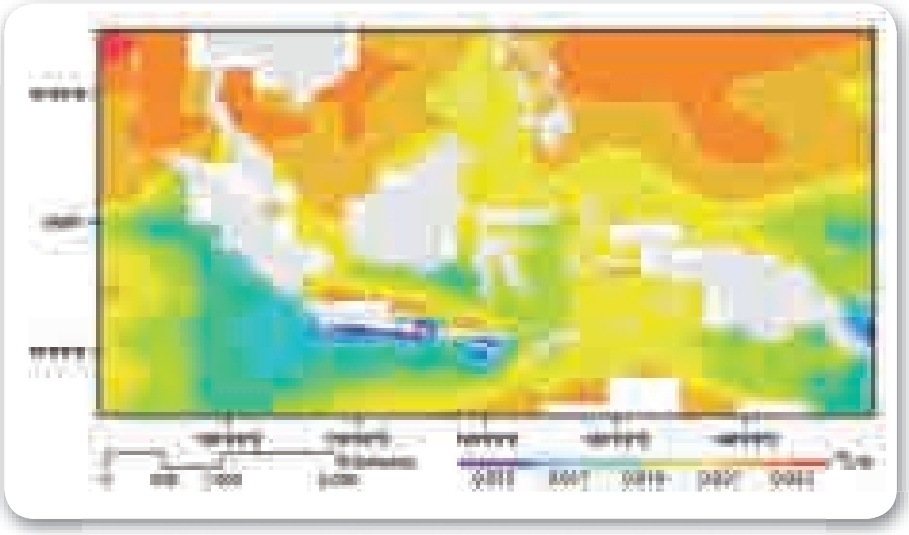

Figure 4. 4 The rate of SST rise based on IPCC SRESa1b, using the MRI_CGCM 3.2 model

Table 4. 1 Projection of the SST increase of Indonesian waters

Item	2030		2050		2080		2100	
SRESa1b	0.65°C	0.65°C	1.10°C	1.10°C	1.70°C	1.75°C	2.15°C	2.20°C
Level of Confidence	High		High		High		High	

Note: sea surface temperature rise is shown with the median, and the bold grey letters shows the estimation of SST rise based on historic data

Finally, high SST rise will affect the potential fishing ground and the damage of coral reefs. The fishing ground probably will move from the tropical area of Indian Ocean, Banda Sea, and Flores Sea, to the sub-tropical areas that remain at lower temperature. On the other hand, if the SST rise rate stays within the adaptive capacity of the reefs and other coastal life forms, then the damaging effects on coastal ecosystems caused by SST rise may be avoided. In addition, as the sea-surface temperature increases, sea level will also rise due to the process of thermal expansion and the adding of water mass from the melting of glacial ice and icecaps in the Greenland, and the Antarctica. The potential sources for sea level rise are depicted in Table 4-2.

Table 4. 2 Potential sources of the sea level rise

Potential source of the sea level rise	
Expansion of sea water volume	0.2 - 0.4 m per °C (Knutti et al., 2000)
Glacier melting	0.15 - 0.37 m (IPCC, 2007)
Icecaps in the Greenland	7.3 m (Bamber et al., 2001)
Icecaps in the West Antarctica	5 m (Lythe et al., 2001)
Icecaps in the East Antarctica	52 m (Rignot et al., 2006)
TOTAL	**± 63m**

4.2 Sea Level Rise Projection

4.2.1 Sea Level Rise Projection based on the IPCC AR4

The average sea level in the Indonesian Seas is shown in Figure 4.5. Generally, the sea level in the Pacific Ocean is 30cm to 50cm higher than that of the Indian Ocean. Sea level in the Java Sea ranges from 20cm to 30cm and 30cm lower than the one over the Karimata Strait. The pattern of Indonesia Through Flow (ITF) can clearly be observed from the characteristics of sea level, forming a lower sea level than that around it, especially the central ITF pathway through the Makassar Strait and point towards the Indian Ocean through the Lombok Strait, the Timor Strait, and the Savu Sea. Even so, the eastern ITF pathway is also visible across the Maluku Archipelago, pointing towards the Indian Ocean through the Timor Strait and the Savu Sea. On the other hand, the western ITF pathway across the Karimata Strait, the Java Sea, and the Lombok Sea cannot be clearly seen. This may be caused by the current of both straits which is mainly influenced by wind, with the depth of 40m to 50m, even though the usual annual current tends to flow towards the Indian Ocean across the Lombok Strait (Sofian, 2008). Details about the seasonal current pattern are discussed in Chapter II.

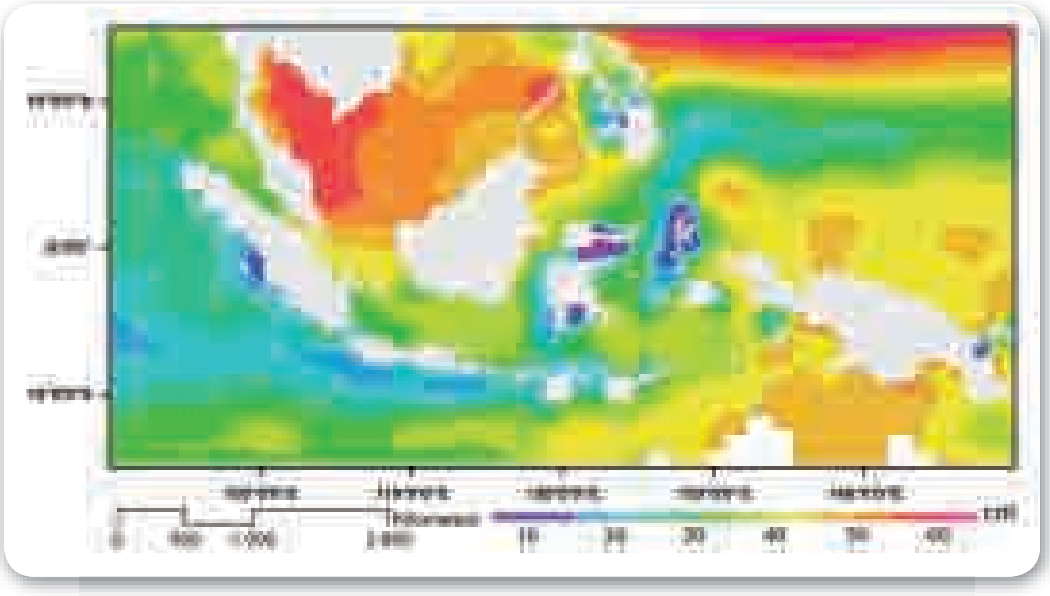

Figure 4. 5 Average sea level rise for 15 years from January 1993 to December 2008, using 0 cm as the lowest regional sea level

Sea level rise due to global warming will bring inevitable consequences. Seasonal current patterns and ITF might be influenced by the changeable rise of sea level, particularly in areas where the rise of Pacific Ocean is greater than that of the Indian Ocean. The eventual geostrophic current pattern will be more dominant than the present one.

Sea level rise not only leads to the changes in current patterns, but also strengthens erosion, coastline

alteration, and the reduction of wetland area in coastal zones. Wetland ecosystems in coastal zones might be damaged if the rise of sea level and SST exceeds the maximum limit of adaptive capacity of coastal life forms. Moreover, the rise of SST also increases the rate of intrusion by seawater into the coastal environment.

To investigate the impacts of global warming on sea level rise rate and its characteristics, the comparative analysis is used to compare the average sea level from 1993 to 2000 with the one from 2001 to 2008. These results can be combined with the use of spatial trend analysis using the data from 1993 to 2008. Figure 4.6 shows the change of sea level based on altimeter data by using the comparative analysis for 7 years. The highest sea level rise rate occurred in the western part of Pacific Ocean with 8 cm rise; the smallest increase occurred in the area off the south coast of Java Island, South China Sea, and the west coast of Philippines near the site of the Mindanao Eddy. Meanwhile, the low sea level rise near the south coast of Java Island is strongly correlated with the thermal expansion caused by temperature in these regions. In general, the differences in sea level rise between the Pacific and Indian Ocean may change the ITF characteristics. These changes will possibly alter the regional climate of Indonesia. The rise of sea level in the Pacific Ocean, which is higher than that of the Indian Ocean, enhances the water transport intensity of warm water from the Pacific to Indian Ocean. Eventually, the increasing intensity of ITF could cause a change in the local rain patterns all over Indonesia.

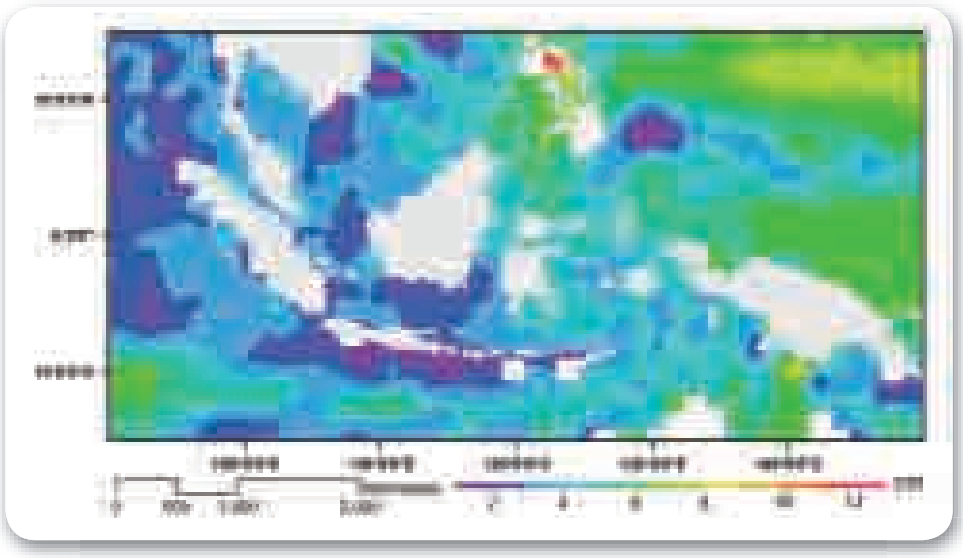

Figure 4. 6 The average magnitude of sea level from 2001 to 2008 subtracted from the average magnitude of sea level rise from 1993 to 2000, with the varying increase of sea level between 2 cm and 12 cm, and the average increase of 6 cm, in 7 years.

The result of spatial trend analysis is shown in Figure 4.7. The SLR rate ranges from 0.2 cm/year to 1 cm/year, with the average around 0.6 cm/year. The highest SLR rate occurred in the Pacific Ocean, north of Papua and reached about 1 cm/year; the lowest occurred close to the south of Java and ranged from about 0.2 cm/year to 0.4 cm/year. If these trends continue, the sea level rise will reach 6 cm to 30 cm in

2030, with the average SLR for all of Indonesia ranging from approximately 15 cm to 18 cm. By 2050, SLR could reach 10 cm to 50 cm, with an average of 25 cm to 30 cm. SLR in 2080 could reach 16 cm to 80 cm with an average ranging from 40 cm to 48 cm. By the end of the century, sea level rise could range from 20 cm to 100 cm, with an average of 50 cm to 60 cm.

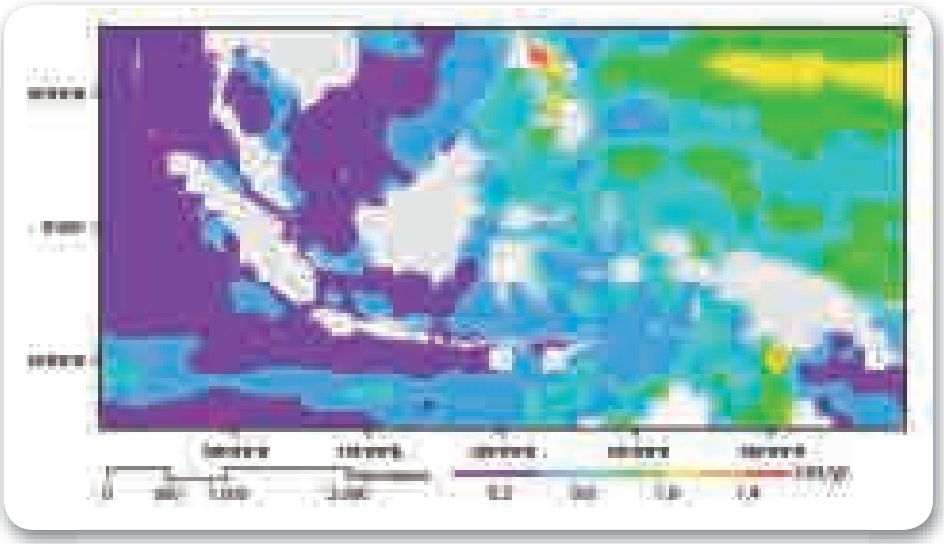

Figure 4. 7 The trend of sea level increase based on altimeter data from January 1993 to December 2008 using spatial trend analysis

The approximated sea level rise using tide gauge data can be seen in Figure 4.8. The rate of sea level rise varies from 0.4 cm/year to 1.2 cm/year, with the smallest rise for the entire region is occurring in Darwin and the highest one is occurring in Manila. The average magnitude of sea level rise of the Indonesian waters ranges from 0.7cm/year to 0.8cm/year. The projection of sea level rise in 2030 suggests about 24 cm ± 16 cm, relative to sea level in 2000. After 2000, the sea level will be expected to rise along with the increase of sea surface temperature. The existing trends suggest that sea level will rise 40 cm ±20 cm and 56 cm ±32 cm, in 2050 and 2080, respectively. If these trends continue, eventually, sea level will rise 80 cm ±40 cm by 2100. In addition, this increase is strongly related with the SST rise. If one assumes that each 1°C increase of SST raises the sea level up to 20 cm to 40 cm, then the sea level will increase 45 cm to 90 cm based on a 2.2°C increase of SST by 2100. The rate of sea level rise based on tide gauge data is relatively similar to that on altimeter data.

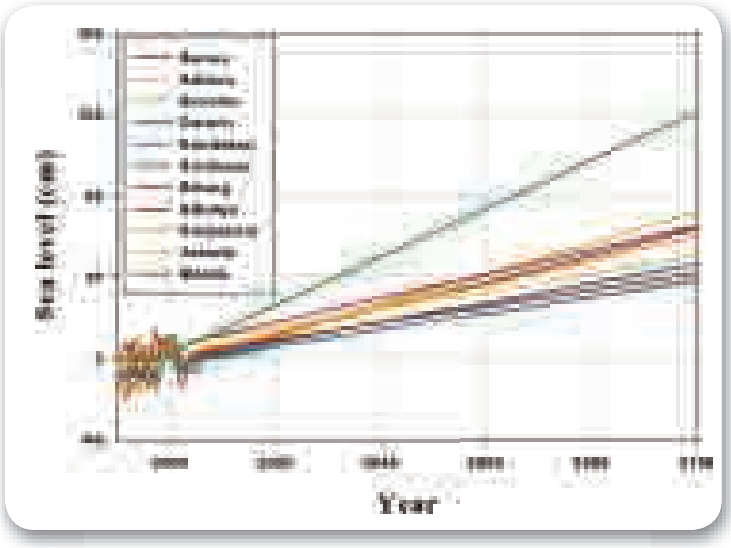

Figure 4. 8 Approximation of sea level rise using a number of tidal data acquired from the University of Hawai'i Sea Level Center (UHSLC)

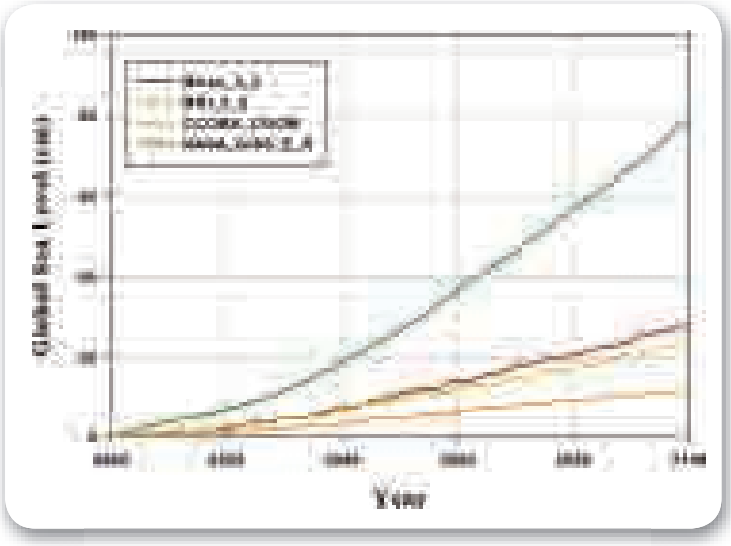

Figure 4. 9 Approximation of global sea level change based on the IPCC SRESa1b assuming CO_2 concentration of 750ppm

Model analysis of the scenarios prepared by the Intergovernmental Panel on Climate Change (IPCC) for the Special Report on Emission Scenario (SRES) indicates that the rate of global sea level rise is projected to vary from 0.2 cm/year to 0.8 cm/year during this century. (See Figure 4.9, picture for SRES A1 and B2 are not shown). The average magnitude of global sea level rise is approximately 0.6cm/year, thus the estimation of sea level rise in the Indonesian waters will be based on the average global increase of 0.6 cm/year. The sea level elevation will be taken from the MRI model version 3.2, illustrating the spatial distribution of sea level rise in the Indonesian waters. The choice of MRI model is based upon the result of model validation, which has been carried out and is explained in the analysis presented in Chapter III.

Figure 4.10 shows the spatial distribution of the sea level rise based on the MRI 3.2 model applied to the global climate described in the SRES A1b scenario. Sea level rise based on the model has smaller projected range than the altimeter-based projection does, although it possesses a relatively similar spatial distribution significant differences occurring only in the northern Indian Ocean. The narrow range of the model-based projections of sea level rise rate might be caused by the low spatial resolution of the global model. The rate of sea level rise is projected to range from 0.7 cm/year to 0.8 cm/year. Overall, average sea level is projected to rise by 22.5 cm ±1.5 cm in 2030 relative to the sea level in 2000. By 2050, the cumulative rise is expected to range from 35 cm to 40 cm. Sea level is projected to continue rising, reaching 60 cm ±4 cm in 2080, and 75 cm ±5 cm in 2100.

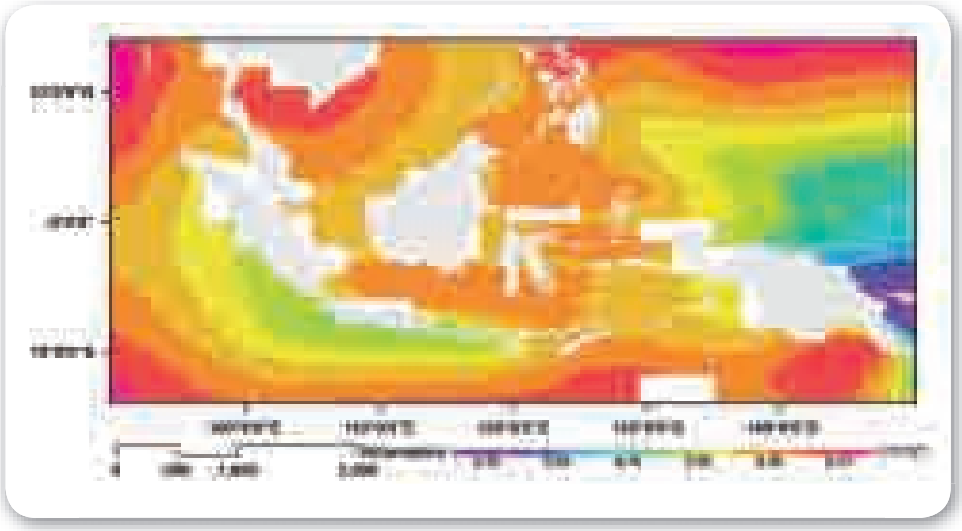

Figure 4. 10 Approximation of the amount of sea level rise in the Indonesian waters based on the scenario of IPCC SRESa1b, assuming CO_2 concentration of 750ppm

The estimation of sea level rise using altimeter, tidal, and model data shows the same trend, with the average rise rates ranging from 0.6 cm/year to 0.8 cm/year. The summary of sea level rise from 2030 to 2100 relative to sea level in 2000 is illustrated in Table 4-3.

Besides affecting the increase of sea level, many scientists predict that sea surface temperature increase in tropical area will increase the frequency of extreme weather events. These, in turn, could increase the frequency of damaging storm surges. This can be observed from the analysis of the potential of El Nino and La Nina based on the IPCC model. (For a more detailed explanation, see Chapter V below.)

Table 4. 3 Projection of the average increase of sea level in the Indonesian waters

Period	Sea Level Rise Projection since 2000			Level of confident
	Tide Gauge	Altimeter ADT	Model	
2030	24.0cm±16.0cm	16.5cm±1.5cm	22.5±1.5cm	Moderate
2050	40.0cm±20.0cm	27.5cm±2.5cm	37.5±2.5cm	Moderate
2080	64.0cm±32.0cm	44.0cm±4.0cm	60.0±4.0cm	High
2100	80.0cm±40.0cm	60.0cm±5.0cm	80.0±5.0cm	High

4.2.2 Sea Level Rise Projection (Post-IPCC AR4)

By using model results, observational data, and the outcome of experiments through 2005, the basic conclusion of the Fourth Assessment Report of the IPCC (AR4) is the increasing concentration of greenhouse gases (GHGs) during the last 50 years has been caused by human activity. These increases of GHG concentration are likely to lead not only to an increase of air and SSTs, but also to an increase of sea level through thermosteric process. Moreover, this increase in concentration caused the increase of global temperature, especially in the Greenland and the Antarctica, and in the central Siberia. In addition, the increase of sea level will range from 20 cm to 80 cm, according to the analysis contained in the IPCC AR4. However, the NASA GISS E_R model projects a 90 cm increase of sea level by year 2100. The IPCC AR4 analysis allocates 70% of this sea level rise to thermosteric processes and 30% to the melting of glacial ice. Meanwhile, the research completed in 2005 has showed an increasing intensity of ice melting, in both the Antarctica and the Greenland.

In general, the temperature rise in the Antarctica is twice that of the global average rise, although the ice models show that part of the highlands of Antarctica are likely to undergo a drastic temperature rise, while other regions experience a drastic temperature drop (UNEP/GRID-ARENDAL, 2007). Besides resulting in ice loss in the Greenland and the Antarctica, the increase of the surface temperature that causes this ice melting will reduce the area of ice-covered surface and will increase the absorption of the sun's short wave by the land and sea. This, in turn, will cause a positive albedo feedback that will accelerate the rate of global warming (see Figure 4.11) which in turn will increase the rate of ice-loss in the Greenland and the Antarctica. Increase of global warming intensity will cause the increasing of SLR rate by thermosteric process.

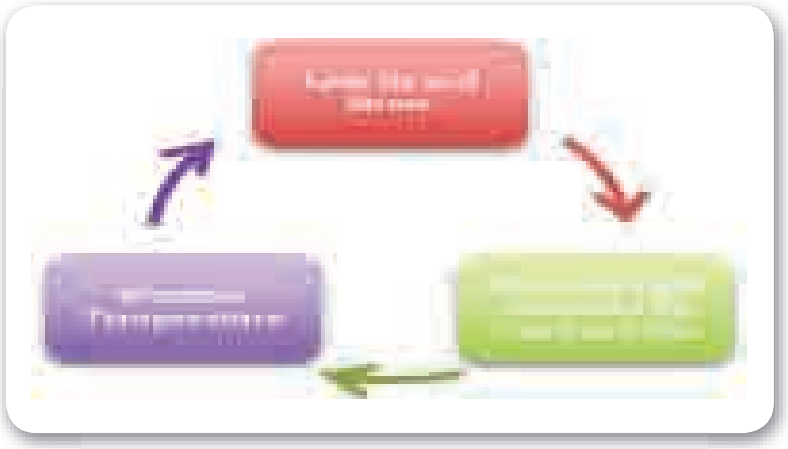

Figure 4. 11 Positive feedback of ice melting and the rising of surface temperature (UNEP/GRID-ARENDAL, 2007)

Figure 4.12 depicts the surface temperature change in the Antarctica for the last 30 years, with the average rise rate ranging from 0.05°C/year to 0.1°C/year. The highest rise rate of surface temperature occurred in the western Antarctica, contributing the potential addition of 6 m to 7 m of sea level, if all surface ice melts. Global sea level rose 1.7± 0.5mm/year until the end of the last century. This is different compared to the global SLR between 1993 and 2003, when the average rate reached 3.1±0.7 mm/year. The change of rise rate indicates the increasing of long-term rise rate variability. This fact indicates that both temperature and ice-lost are contributing to the SLR. However, the model and IPCC AR4 approximation shows no indication of dynamic alteration of ice melting.

The IPCC AR4 projection is based upon the mass difference of ice melted and ice formed. Since the mass of the melting ice is bigger than that of the ice forming, the Greenland ice sheet does contribute to the rise of sea level (Ridley, et al., 2005). On the contrary, Antarctica is projected to freeze more and undergo increasing ice forming, thus the ice forming in the Antarctica and the ice melting in the Greenland will cancel each other, with no net contribution to the sea level rise. Thus most of the contribution to the changing mass (the difference between ice melted and ice formed) is limited to the melting of glaciers and mountain ice cover (Meehl, et al., 2007).

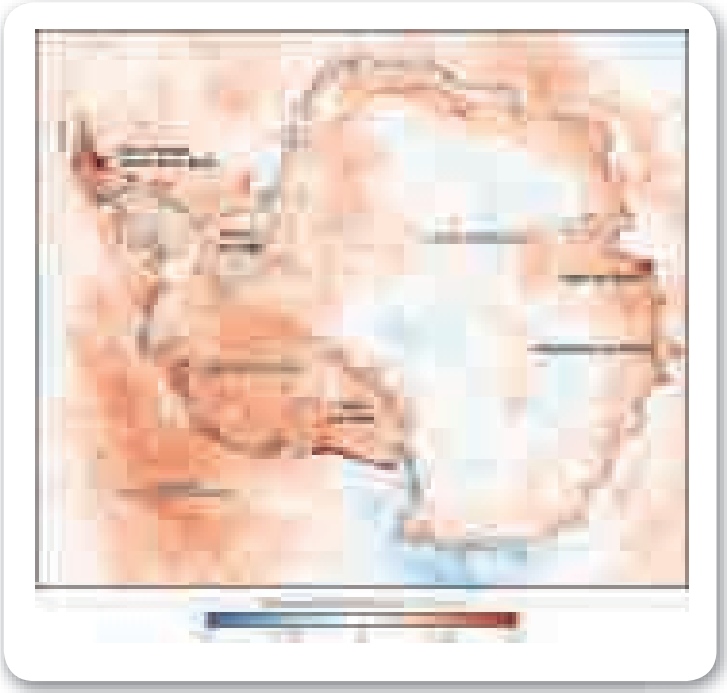

Figure 4. 12 The change in Antarctica's temperature in the last 30 years
(Source: Earthobservatory, NASA, 2007)

Rahmstorf (2007) use the relationship between the rise of the sea level and surface temperature to predict the sea level rise in the end of the 21st century. His estimate ranges from 50 cm to 140 cm, relative to the sea level in 1990. This prediction is higher than the projection of IPCC AR4. Moreover, the sea level rise before 1990, due to mass changing, is purely dominated by the glacial melting (Bindoff, et al., 2007), thus Rahmstorf's prediction (2007) excludes the changing of sea level due to the ice melting in the Antarctica and the Greenland.

The ice melting in the Greenland happened since the midst of 1990s, whose melting acceleration increases from time to time (see Figure 4.13). Even though the ice elevation on highlands keeps increasing due to the snow, the ice melting in coastal areas and lowland is much greater and more intensive. The rate of ice melting in the Greenland reaches 100 Gigatons per year (Gt/year) by the end of 1990s, increasing to an observed rate of 200 Gt/year by 2006 (Steffen, et al., 2009). (Approximately 360 Gt of ice melting is equivalent to a 1 mm increase in sea level.) The rate of ice mass change in the Antarctica reached 80 Gt/year during the 1990s, and increased to 130 Gt/year by 2006. These changes cause the increasing rate of sea level rise, and will lead to a total increase of sea level of 140 cm to 180 cm. Projections of the global sea level rise in 2100 are illustrated in Figure 4.14 below.

Figure 4. 13 The change of the ice-covering layer of Greenland based on analysis using IceSAT satellite (source: Earthobservatory, NASA, 2007)

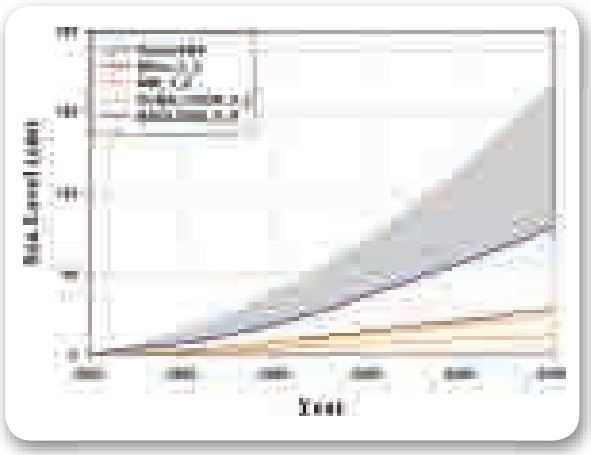

Figure 4. 14 The sea level rise until year 2100, relative to sea level in 2000

By using the post AR4 sea level rise projection, spatial distribution of the rate of sea level can be illustrated in linear form as in Figure 4.15. According to Figure 4.15, sea level rise will reach 175 cm in 2100 relative to the level in 2000. Sea level will reach 52.5 cm in 2030, 87.5 cm in 2050, and 140 cm in 2080. This leads to an increasing frequency of abrasion, erosion, and seawater inundation that is not only caused by the high sea level, but also by the high wave and tidal, which is modulated by the high sea level, particularly during the La Nina events.

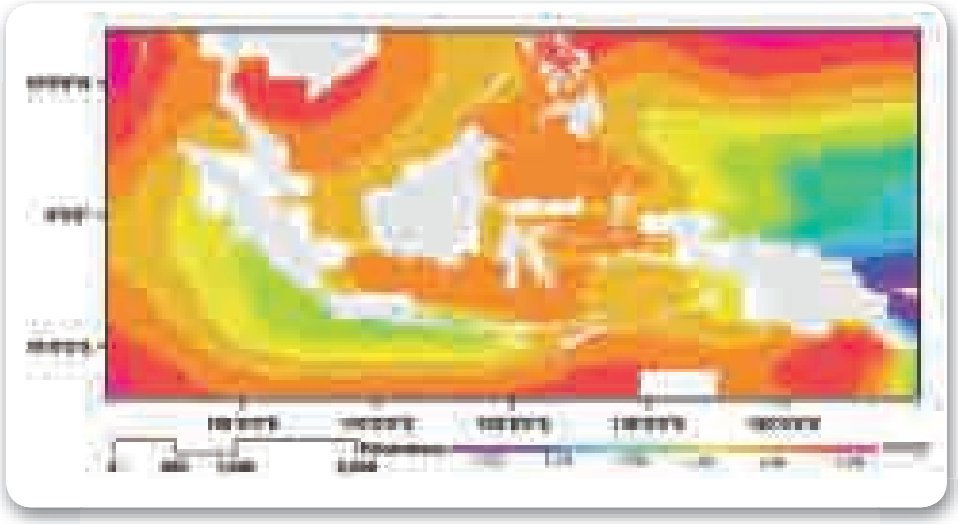

Figure 4. 15 Estimated rate of sea level rise in the Indonesian waters, based on model projections plus dynamic ice melting, post IPCC AR4

5

EL NIÑO AND LA NIÑA PROJECTIONS

It cannot be denied that in the last few decades, many natural disasters have occurred, including coastal floods, ship accidents and tidal waves caused by extreme weather events. The extreme weather conditions, possibly associated with El Niño and La Niña in the Pacific Ocean along with the Indian Ocean Dipole Mode (IOD) in the Indian Ocean, have direct effects on coastal zones and marine transportation, as well as indirect effects on the forestry, agriculture, health, and land transportation sectors, through changes in rainfall caused by extreme weather.

Many oceanographers believe that with the increasing intensity of global warming, the intensity of extreme events such as El Niño and La Niña (usually known as ENSO, or the El Niño-Southern Oscillation, comprising both El Niño and La Niña) will increase as well. ENSO is a natural phenomenon occurring every few years, because of the evolution of SST in the tropical Pacific Ocean. El Niño is marked by the decrease of SST in the Indonesian waters, and an increase of more than 0.5°C in the eastern tropical Pacific Ocean. As a consequence, the air pressure in Indonesia rises, causing the Pacific trade wind to weaken and easterly local winds to strengthen, although, in the early phases of El Niño, westerly local wind bursts are also known to happen. The decreasing of SST and the shifting of the warm-pool from the Indonesian waters to the central tropical Pacific Ocean, cause a decrease in rainfall in most of Indonesia. This, in turn, increases the risks of forest fires and drought, especially in the eastern Indonesia. On the other hand, La Niña is a natural phenomenon with dynamics and impacts that are opposite to El Niño.

La Niña is marked by the rise of SST in the Indonesian waters, and the fall of SST in the eastern tropical Pacific Ocean by more than 0.5°C. In the La Niña period, the Pacific trade wind becomes more intense, which causes the warm-pool to shift to the west compared to normal conditions. This warm-pool westward shifting causes more intense rainfall in Indonesia, and therefore increases the dangers of flooding.

Aside from forest fire and flood risks, ENSO can also assist in causing tidal waves and tropical storms, which may cause coastal flooding and marine transportation accidents. An illustration and the mechanism of the sea transportation accidents that have happened lately can be seen in Figure 5.1.

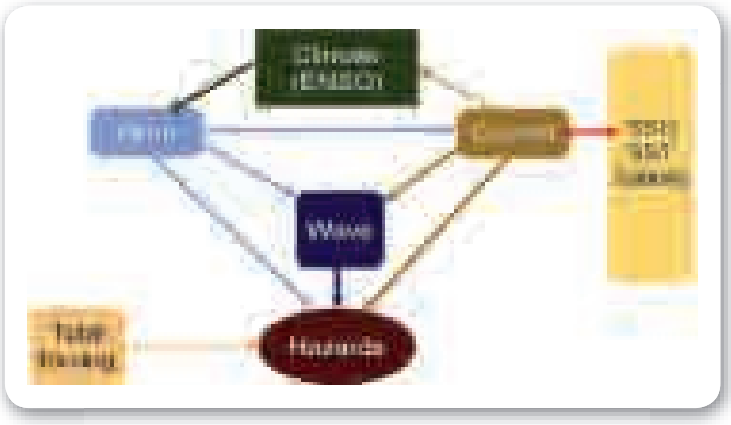

Figure 5. 1 An illustration of the scheme and causes of marine transportation accidents in the last few decades. SSH and SST indicates the sea surface height and sea surface temperature respectively.

Many of the sea transportation accidents that have occurred recently were caused by high waves and ocean winds resulting from extreme weather (e.g., the KM Senopati disaster on December 29, 2006, and the KM Teratai Prima on January 11, 2008). However, other factors such as tidal and wind-induced surface currents were also involved in these accidents.

5.1 Global Warming and ENSO

The ENSO phenomenon is based on the changing patterns of ocean surface temperatures in the Pacific Ocean. Therefore, the frequency of El Nino and La Nina can be estimated using the data of Nino3 (the region of the eastern Pacific Ocean spanning from longitude 210°E to 270°E and from latitude 5°S to 5°N) SST, by using wavelet analysis. The SST data of Nino3 is in turn obtained from MRI models. (The choosing of model is based on climatologic comparisons of the most realistic sea levels in the case study in the Lombok Island, Figure 5.2). The SST data of Nino3 used are monthly anomaly data.

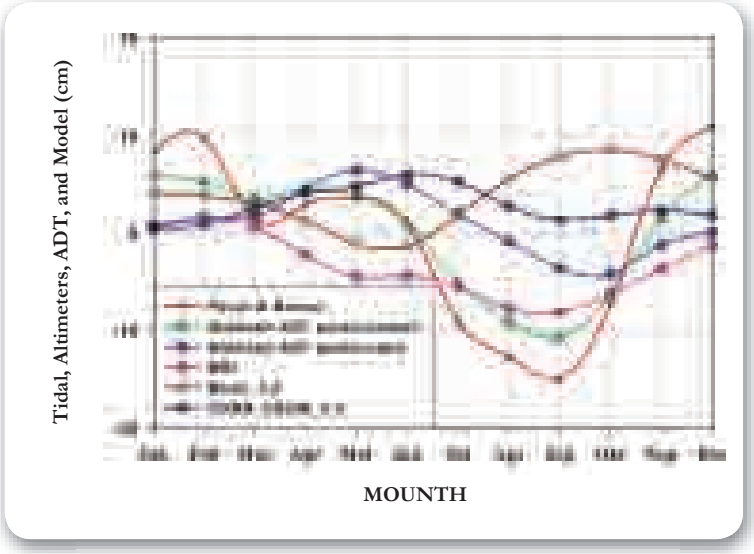

Figure 5. 2 Sea level climatology based on tidal gauge, altimeter, and IPCC model data. Model data were only displayed by sea level at the southern coast of Lombok Island.

Figure 5.2 shows the sea level climatology with tidal gauge, altimeter, and IPCC model data. The MRI 3.2 model shows a sea level estimation, which is more realistic compared to the highest yearly sea level occurring in January to February, and the lowest occurring in August to September. The Absolute Dynamic Topography (ADT) altimeters on the southern coast of Lombok showed the same pattern as the estimation of MRI 3.2 with the highest sea level occurring in January to February and the lowest occurring in August to September. Meanwhile, the tidal gauge data in Benoa, Bali, also showed the same yearly fluctuation pattern although with a higher sea level amplitude. The highest sea level occurs at 15 cm and the lowest sea level at -15 cm. From these sea level characteristics, the MRI 3.2 model is considered more realistic and can be used to predict the frequency of the occurrence of El Nino and La Nina for the next 100 years.

Figure 5.3 shows the results of the wavelet analysis using historic data from 1871 to 1998. Based on the historical data of Nino3 SST from 1870 to 1998, it has been shown that ENSO occurs every two to seven years, with an intensive ENSO period occurring from 1875 to 1885 at the beginning of the industrial revolution in Europe. The second ENSO period occurred in 1900 to 1920, during the First World War. The third period occurred from 1920 to 1939, with a frequency of one to two years. This is correlated with the mass industrialization put in action, especially by the defeated nations in the First World War, followed by the ENSO period from 1939 to 1945 with a one-year frequency for five years. The ENSO phenomenon entered a relaxing period from 1945 to 1965, which was followed by the fourth period from 1965 to the present day. The increasing frequency of ENSO since 1965 is caused by the development of Third World countries, changing from agrarian to industrial countries. After 1965, the ENSO period has risen to once every two to six years with a longer length of time. The total power spectrum energy shows that the ENSO with a frequency of four years has the highest energy (see panel c). This shows that from 1870 to 1999, the average frequency of the occurrence of ENSO is around four years.

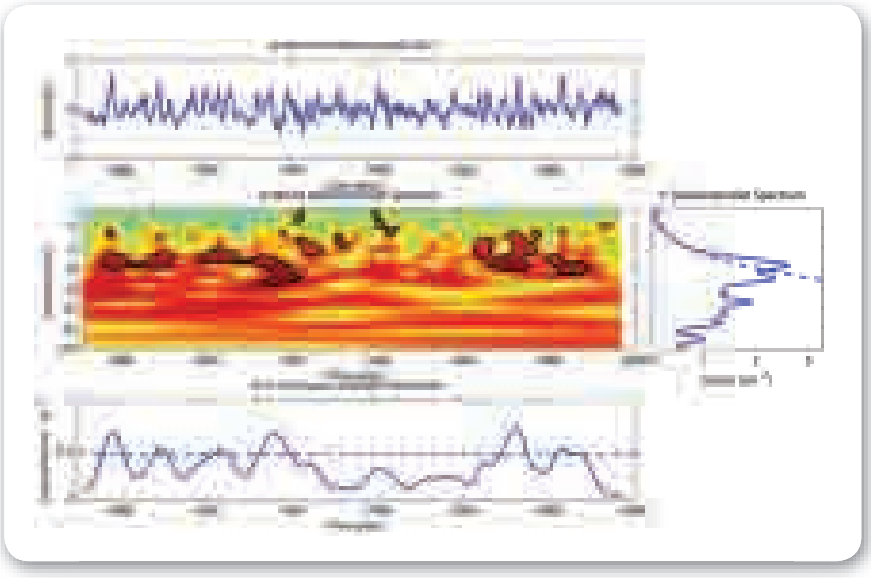

Figure 5. 3 Result of wavelet analysis for historic data from 1871 to 1998.
The dC indicates the degree Celsius

Figure 5.4 shows the time frequency analysis using wavelet transformation for the MRI model data from 2001 to 2100 based on the SRES a1b scenario. Figure 5.4 panel b shows that El Nino and La Nina occur with a period of every two or three years. Meanwhile, the largest El Nino and La Nina are projected to occur from 2115 to 2015, 2015 to 2025, 2050 to 2055, and 2065 to 2070. In addition, based on global wavelet power spectrum data, Figure 5.5 panel c illustrates that the average frequency of ENSO could be every two or three years. The average energy spectrum in the SRES A1b scenario is higher than the historic data (Figure 5.3). The occurrence of El Nino will be followed with the occurrence of La Nina as shown in the Nino3 time series. This transition period causes drastic changes in sea water levels up to

20 cm. Aside from the rising sea levels; extreme climate conditions will cause extreme weather that may lead to additional high waves.

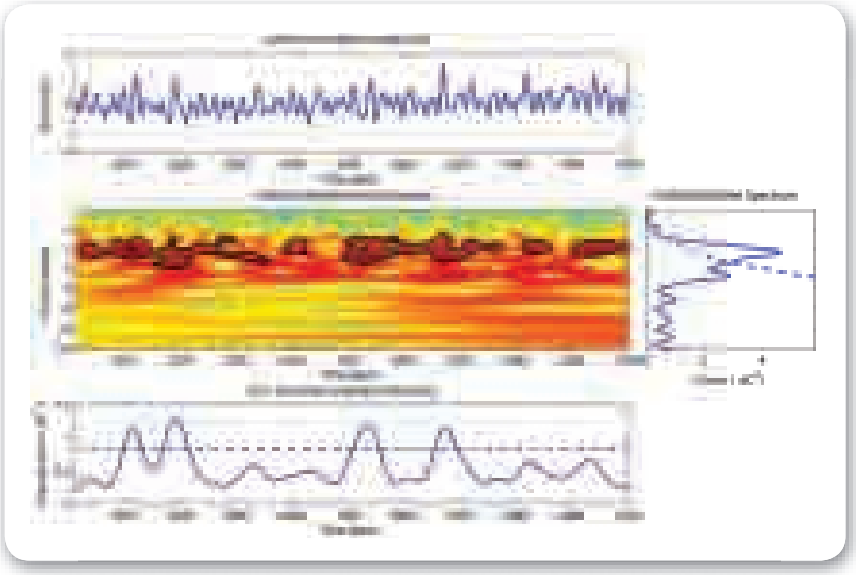

Figure 5. 4 Wavelet analysis results for the SRESa1b scenario. The dC indicates the degree Celsius

Figure 5.5 shows the result of wavelet analysis applied to the SRES A2 scenario. This analysis indicates the largest El Nino and La Nina events are projected to occur from 2045 to 2050, 2060 to 2065, and 2075 to 2085. The energy spectrum of SRES A2 is lower than the SRES A1b scenario in the period prior to the year 2050, although ENSO still occurs every three years. (See Figure 5.4 panel c.) But the strength of the ENSO dynamic is lower than that in the SRES A1b scenario. The average frequency of ENSO in this scenario is once every four years, based on global spectrum data (panel c). However, the frequency of ENSO increases drastically after 2060. (See Figure 5.4, panel d).

Figure 5.6 shows the results of wavelet analysis applied to the SRES B1 scenario. The largest El Nino and La Nina occur in the scenario from 2035 to 2040, with a higher ENSO strength compared to the other two scenarios. Based on global spectrum data, the SRES B1 spectrum energy is lower than the other two scenarios, with ENSO occurring every three to four years. (See panel c.) An example of the calculations using the MRI output model for Nino3 SST for the estimation of the occurrence and frequency of ENSO are shown in Table 5-1 below.

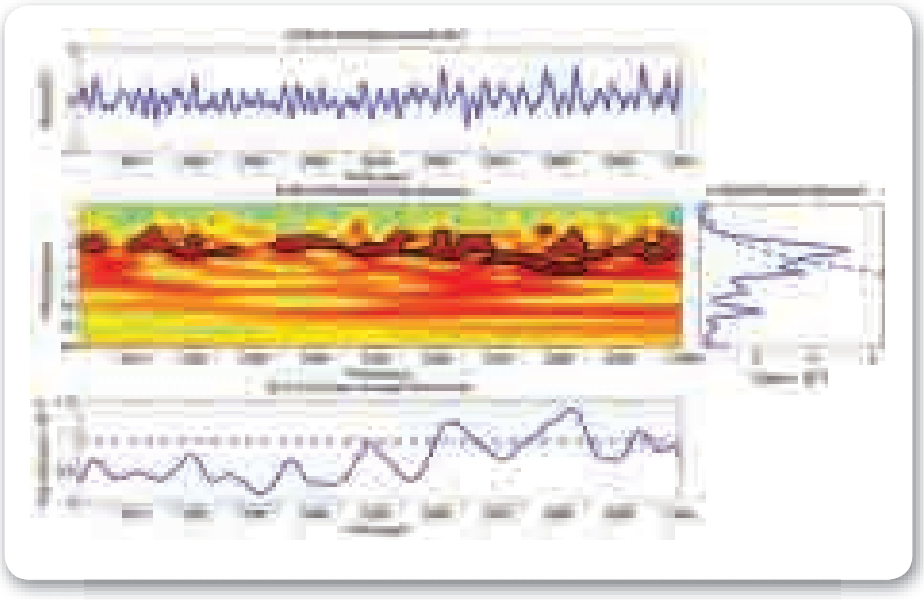

Figure 5. 5 Wavelet analysis results for the SRESa2 scenario. The dC indicates the degree Celsius

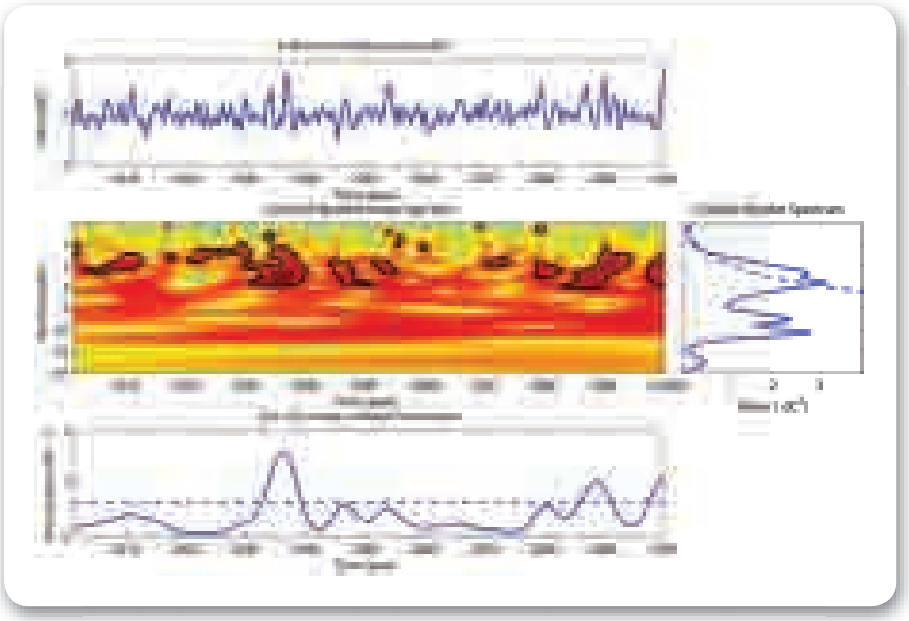

Figure 5. 6 Wavelet analysis results for the SRESb1scenario. The dC indicates the degree Celsius

Table 5-1 shows the frequency (timetable) of the occurrence of ENSO from 2001 to 2030, based on the SRES A1b scenario. The timetable is based on Nino3 monthly SST anomaly. The chances of the occurrence of ENSO comprising of La Nina and El Nino, happens almost every year with a normal period occurring in three years, namely in the years 2013/2014, 2021/2022 and 2027/2028.

Table 5. 1 ENSO timetable based on the MRI model output

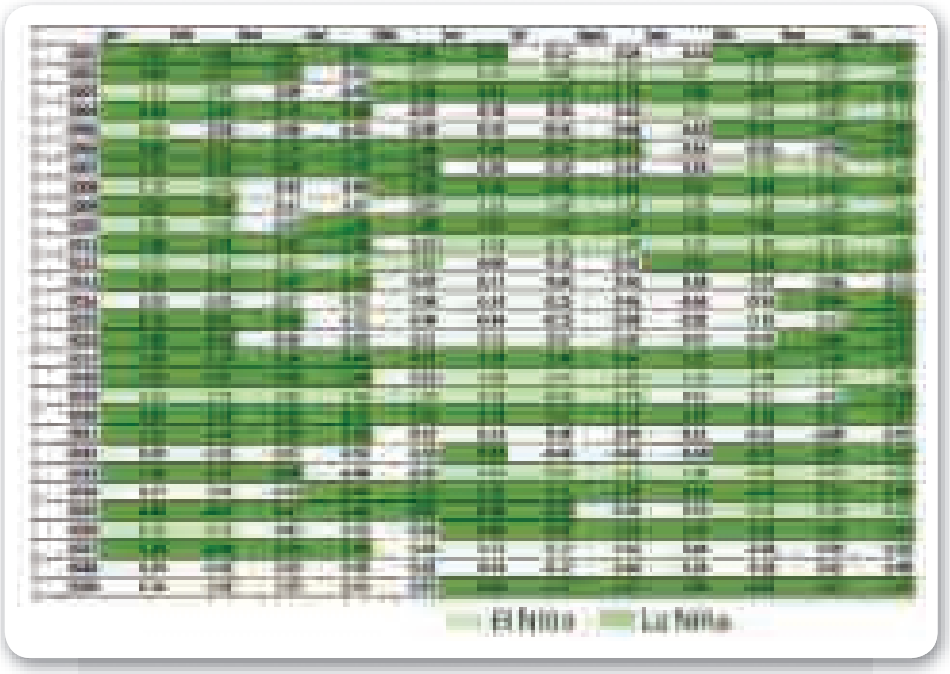

5.2 ENSO and Sea Level Variations

5.2.1 ENSO and Mean Sea level

Using HYbrid Coordinate Ocean Model and tidal gauge data from Jepara, Jakarta, and Surabaya, Sofian (2008) discovered that ENSO influence is still clearly seen using the model and tidal data. Both model and tidal data show a drastic and rapid increase during the transitional period between strong El Niño (1997/1998) and strong La Niña (1998/1999). However the model estimates tends to be lower than the observed tide in Jepara and Surabaya.

Figure 5.7 shows the time-series of altimeter sea level anomaly from year 1993-2008. Monthly sea level anomaly is calculated based on the weekly mean sea level at longitude 90°E to 150°E and from latitude 5°N to 5°S, relative to sea level climatology. During El Niño, sea level will be depressed up to 20 cm below normal, and during La Niña it will be elevated by 10 cm to 20 cm. This affects the risk of erosion, abrasion, and seawater inundation, particularly during La Niña, which brings higher rain intensity. Sofian et al. (2007) posted that sea level rise during the transitional period of El Niño and La Niña, and during La Niña was caused by strengthening trade wind in the Pacific Ocean that brings water mass from the East Pacific near Peru to the Indonesian Water. These transitions are marked by displacement of the warm pool from the Central Pacific Ocean to the Indonesia Sea. This causes an increase in sea level gradient so that the sea level in the Indonesian seas is 1 m higher than the sea level of the Eastern Pacific, for example, in and around Peru. Nevertheless, the local wind tends to be westerly wind because the decline of air pressure in Darwin and the Indonesian Water tends to decrease the sea level in the Indonesian Water.

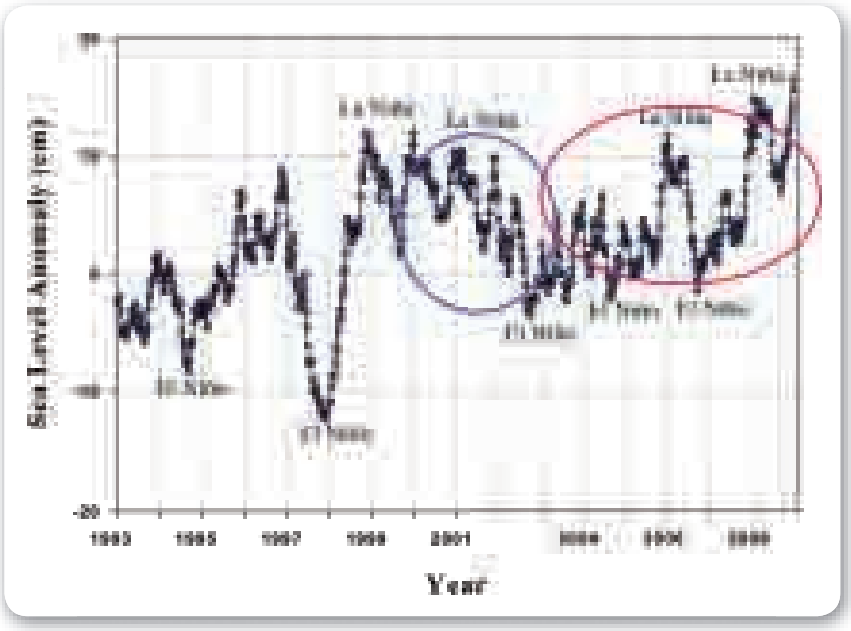

Figure 5. 7 Time series of altimeter sea level anomaly from 1993 to 2008. Sea level anomaly falls to 20 cm during strong El Niño, and rise 20 cm during strong La Niña

In addition, it is also clearly seen that sea level is highly rising and reaching up to 20 cm from year 1993 to 2008 (although there is a sea level anomaly drops from 1999 to 2004). Since 2004, the sea level rise has been in rebound with a higher acceleration rate. This is noticed by the rising value of sea level during El Niño. Moreover, the influence of geographical location to sea level rise can be seen in Figure 5.8.

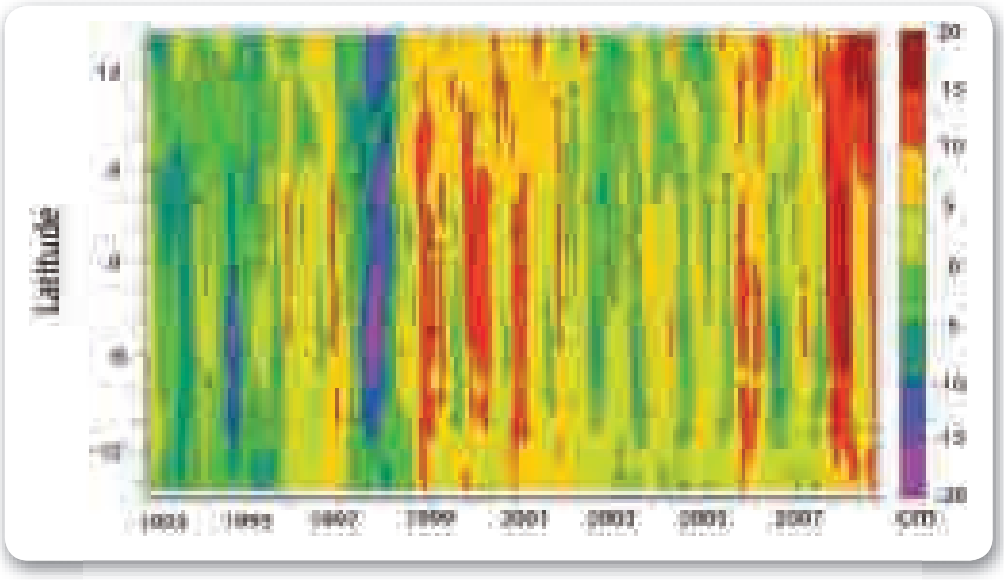

Figure 5. 8 Hovmoller diagram of time-latitude sea level anomaly from 1993 to 2008, with the lowest sea level anomaly in 1997/1998 during strong El Niño and the highest in 2008 during La Niña

Figure 5.8 shows the Hovmoller diagram of sea level anomaly in the Indonesian Water from 1993 to 2008. This diagram displays average sea level anomaly from longitude 90°E to 150°E against the latitude. Based on the Hovmoller diagram in Figure 5.8, the Indonesian Waters located from latitude 10°S to 15°S have a small sea level oscillation compared to the other regions, with the highest sea level anomaly in 1999 and 2006, and ranging from 10 cm to 15 cm. On the other hand, the lowest sea level anomaly occurred during moderate and strong El Niño between 1993 to early 1998, with a range from -10 cm to -5cm. The Java Sea, Karimata Strait, southern South China Sea, Banda, Flores, and Aru Sea, that are located from latitude 10°S and 8°N, have the lowest sea level anomaly that reached to -20 cm in 1997 to 1998, and the highest, reached 20 cm, during January to April 2008.

The northern part of South China Sea and north of Papua, have the highest sea level anomaly with low oscillation level, ranging only from -5 cm to 20 cm. From the abovementioned conditions, it can be concluded that the areas around the equator from latitude 10°S to 8°N is strongly affected by the ENSO in comparison to other regions.

5.2.2 ENSO and Extreme Waves

Generally, the distribution of yearly average significant wave height (SWH) in the Indonesian waters can be seen in Figure 5.9. This figure shows the highest SWH in the Indian Ocean. The average SWH in Java Sea is reaching approximately 0.6 m to 1.2 m. The wave height in the southern part of Karimata Strait, Makassar Strait, Banda Sea and Flores are relatively low, with an average about 0.6 m to 1 m. By contrast, the wave height around the Papua Island is about 1 m to 1.4 m.

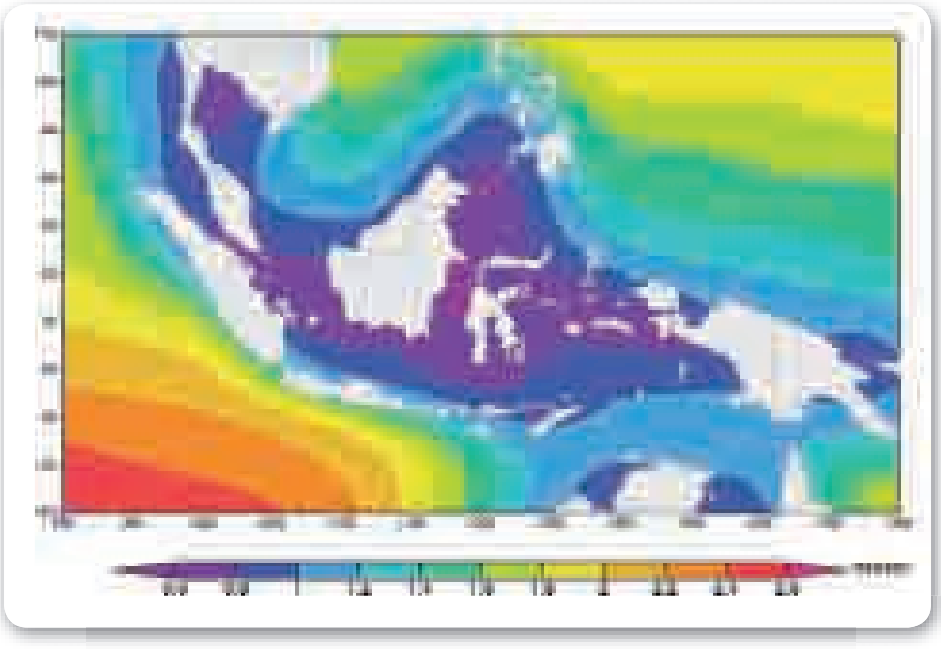

Figure 5. 9 Average significant wave height processed from altimeter data from 2006 to 2008

Figure 5.10 shows the Hovmoller time-latitude diagram of daily wave height in the Indonesian waters from October 11, 2005, until March 4, 2009. The figure illustrates the average wave height on the longitude 90°E to 150°E against latitude. Figure 5.10 shows that the wave height in the Indian Ocean is inversely proportional with the wave height on the north side of equator line in the Indonesian waters. The wave height in the Indian Ocean increases in April to October and tend to decrease in November to March. The Karimata Strait and Makassar, along with the South China Sea and Sulawesi, have the highest annual wave height during the northwest monsoon from October to March and the lowest annual wave height during the southeast monsoon from May to September.

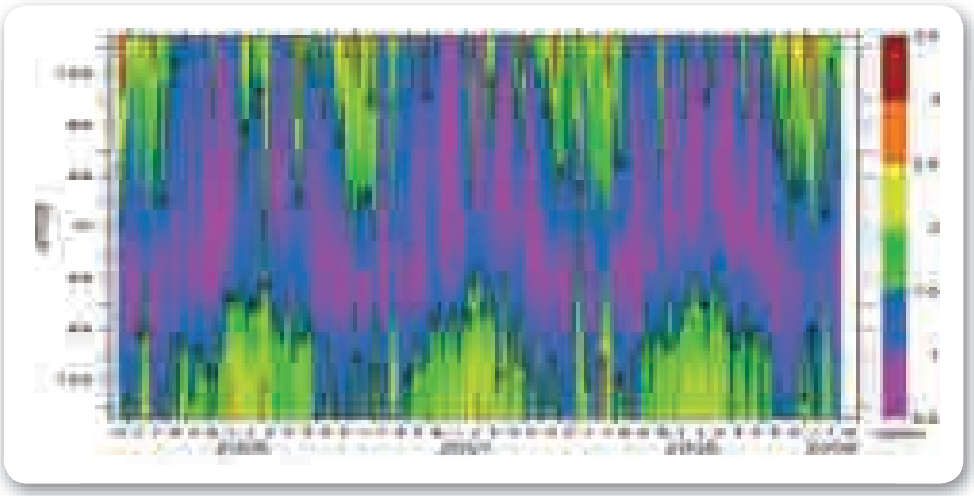

Figure 5. 10 Hovmoller Diagram of daily time-latitude Significant Wave Height (SWH) with the lowest SWH happening in the area at 8°S to 4°N, also SWH height is inversely proportional between SWH in the South China Sea, Pacific and Sulawesi Sea (between latitude 4°N to 12°N) with SWH in the Indian Ocean (between latitude 8°S to 12°S)

On the other hand, the maximum SWH occurs during extreme waves because of the increase in wind forcing, as seen in Figure 5.11. Besides, the spatial distribution of average wave height in the Indian Ocean is higher than the average wave height in the Pacific Ocean north of Papua Island, although the extreme wave in the Pacific Ocean is 1 m to 2 m higher than the extreme wave in the Indian Ocean. During the occurrence of extreme waves, there is an increase of wave height of about 1.5 m almost in all parts of Indonesian waters, including in Java, Sulawesi, Banda and Flores Seas, also in the Karimata and Makassar Strait compared to the annual average wave height. (See Figure 5.9 above.)

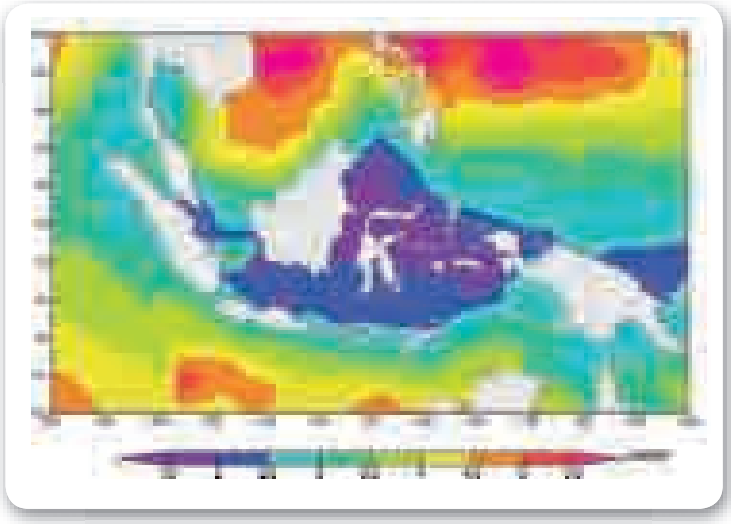

Figure 5. 11 Maximum significant wave height during extreme wave, processed from the altimeter data of significant wave height from 2006 to 2008

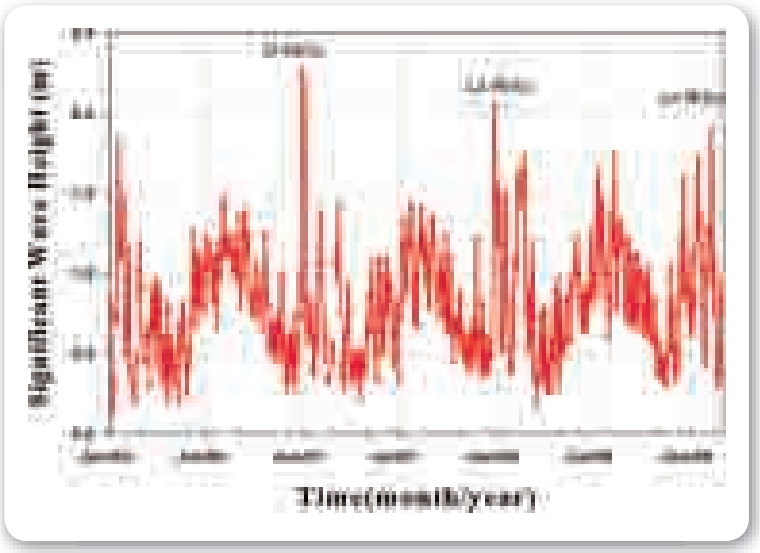

Figure 5. 12 Time-series of wave height from January 1st 2006 to March 1st 2009 in the Java Sea

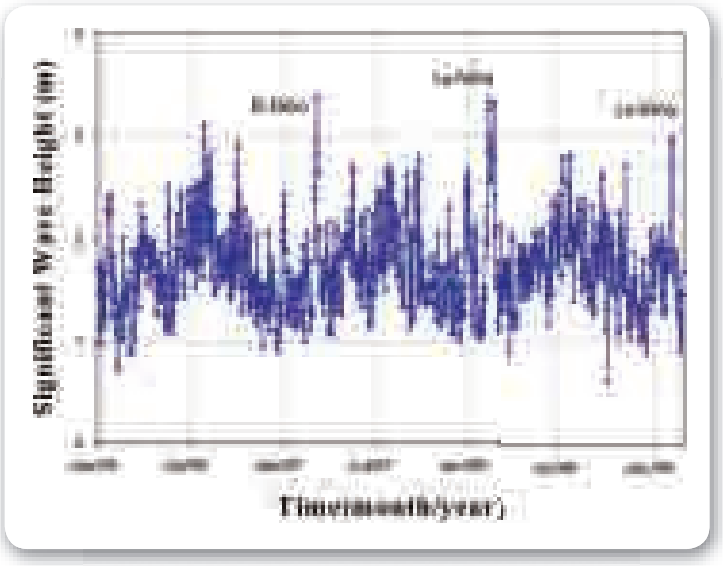

Figure 5. 13 Time-series of wave height from January 1st 2006 to March 1st 2009 in the southern of Java Island

Extreme waves that occur as a result of extreme events may cause sea transportation disasters. Figure 5.12 and 5.13 shows how extreme events such as La Niña and El Niño can cause a wave with variation between 2.1 m and 2.5 m in the Java Sea, and 3 m to 3.5 m in the southern part of Java Island. This occurs even though El Niño does not impact significantly on the wave height along the southern coast of Java. During El Niño, the air pressure in Darwin increases and causes a decrease of westerly wind speed, but wind bursts (i.e., the momentary impulse of high velocity westerly wind that occurs due to low and unstable SST in Indonesia) often happens in open seas during this period and rarely happens in semi-enclosed regions like the Java Sea. (See Figure 5.14). Anomalies in the wind pattern with two vortex in the Western Kalimantan and Australia can occur during this period, causing high-velocity pulses of western wind in the Java Sea to reach 20 m/s. Increasing wave height in the Java Sea, on December 29th 2006, such a high-velocity pulse occurred, increasing the wave height in the Java Sea and causing the KM. Senopati to sunk, killing more than 200 passengers on board.

In addition, the high wave height during El Niño and La Niña phases will increase the intensity of erosion and abrasion, with a high level of damage. In the end, a higher intensity of El Niño and La Niña can intensify changes in shoreline, although the sea level rise is only 1 cm/year.

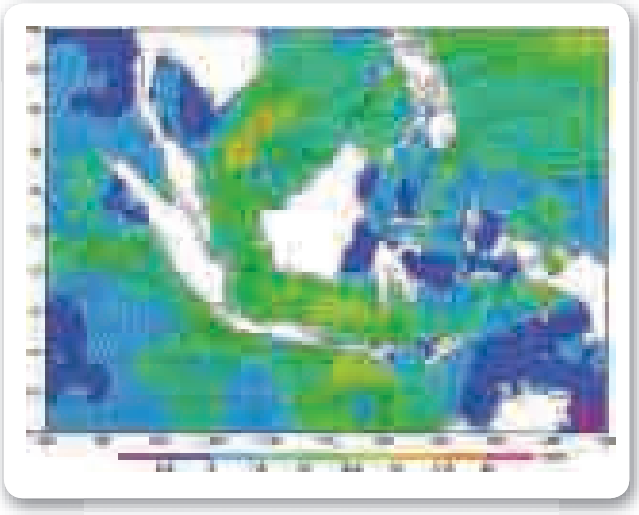

Figure 5. 14 Wind speed and direction on December 29th 2009

5.3 ENSO, Sea Surface Temperature and Chlorophyll-a

The displacement of the warm-pool is a good indicator of the multiyear phenomena, El Niño and La Niña. This displacement brings impacts to sea surface temperature in the Indonesian waters. From climatological data (see chapter III), it is known that in August to October during the southeast monsoon, the concentration of chlorophyll-a off the southern coast of Java Island, Nusa Tenggara, southern Sumatera, Ambon and Sulawesi increases, reaching 0.4 mg/m^3 as the result of upwelling caused by easterly wind propagation. On the other hand, the sea level temperature reaches its annual lowest point, between 26°C and 27°C.

In general, the fishing grounds are influenced by SST and chlorophyll-a concentration (Hendiarti et al., 2005). The fishing ground potential of the area will increase when the SST is low and the concentration of chlorophyll-a is high as the result of the upwelling that lifts nutrients from deeper layer (100 m to 200 m). These effects combine with lower temperature resulting from the Ekman Pumping effects that is caused by coriolis force and easterly wind. The upwelling intensifies during each El Niño. In addition, there are other areas where upwelling occurs because of local Ekman transport, especially in water bodies surrounding the Banda Sea and Flores Sea. On the other hand, the high concentration of chlorophyll-a off the southern Papua coast may not indicate upwelling, but instead illustrate the intensity of abrasion and the turbidity of the sea, as it depth does not exceed 50m.

El Niño and La Niña as a global phenomenon that affects the upwelling and downwelling process will eventually create changes and shifting of fishing grounds. Figure 5.15 shows SST anomaly in August and September from 1980 to 2008. Based on the SST pattern in August and September from 1980 to 2008, it can be concluded that there is a decline of production from fish catching during La Niña due to the high SST, and an increase in fish production during El Niño due to the decline in SST.

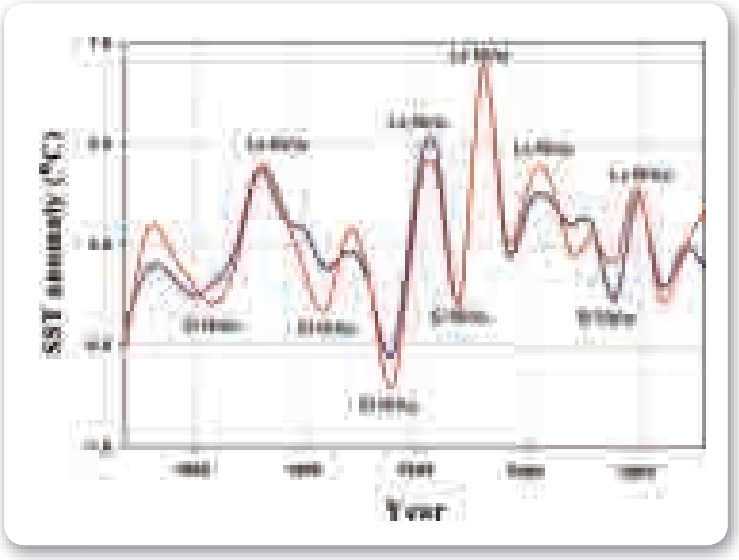

Figure 5. 15 SST anomaly from 90°E to 150°E and from 15°S to 15°N on August and September year 1980 to 2008. The increase of SST of more than 0.35°C shows strong La Niña period, and decrease of 0.35°C shows strong El Niño

a. September

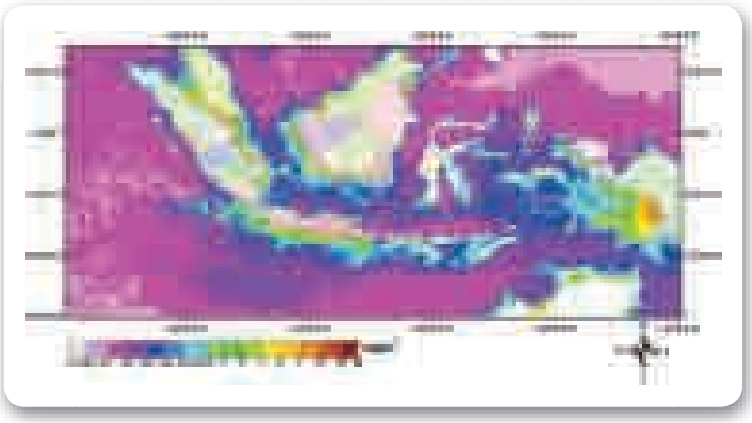

b. September 1997

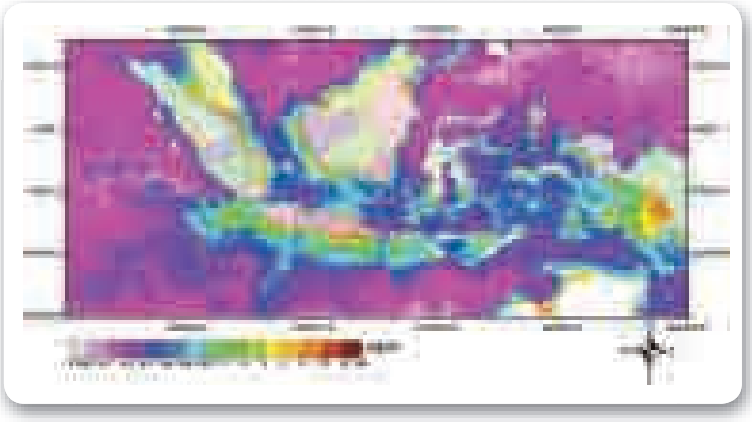

c. September 2008

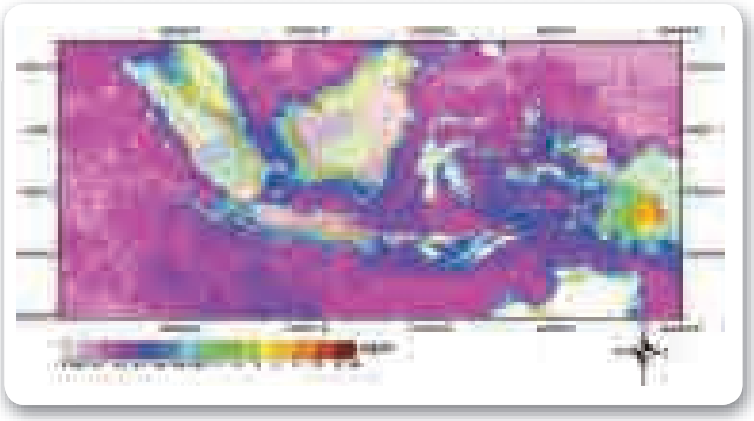

Figure 5. 16 Chlorophyll-a distribution on September during normal condition, El Niño and La Niña

Spatial distribution of chlorophyll-a is shown in Figure 5.16, displaying distribution during (climatological) normal, El Niño (September 1997) and La Niña (September 2008). During normal condition, the chlorophyll-a in the southern coast of Lombok, Java, Bali, and parts of Sumatera, Banda Sea and Flores Sea reaches 0.4 mg/m3. The increase of chlorophyll-a concentration occurs during El Niño as the result of strengthening easterly wind caused by increasing air pressure in Darwin and the Indonesian waters. The strengthening of easterly wind causes the strengthening of Ekman Pumping and the intensification of upwelling in southern coast of Java, Bali, Lombok Island and some parts in Sumatera (September 1997). It also causes local Ekman transport in Banda and Flores Sea.

During El Niño period, based on chlorophyll distribution, the fishing ground area are spread along southern coast of Java, Bali, Lombok, and some parts of Sumatera, as well as the Banda and Flores Sea. On the other hand, during La Niña, the air pressure in Darwin declines and causes the easterly wind during southeast monsoon to weaken. The upwelling process does not occur well and causes the lower mixing depth, lessening nutrient and phytoplankton growth as seen in Figure 5.7b. This, aside from the influence of increasing sea surface temperature causes the declining yields from these fishing grounds. In addition, the fishing grounds that still have better potential are the water bodies near the Sumbawa Island, Timor, and the southern coast of Java Island which still have high concentrations of chlorophyll-a.

5.4 ENSO and Coral Bleaching

Indonesia is a maritime country that is rich with biological resources in its seas; particularly its coral reefs. Coral reefs are very vulnerable to abrupt change of temperature. In general, coral reefs can live well in temperature between 26°C and 30°C. However, an increase of SST between 1°C and 2°C from the mean annual value can trigger coral bleaching. (Hoegh-Guldberg, 1999; Coles and Brown, 2003) A significant increase in SST can cause coral bleaching in a short time, as little as 2-3 weeks. Meanwhile, the decline in SST needs a longer time to bleach the coral reef. The identification of area with coral reef damage due to bleaching based on sea surface temperature can be seen in Figure 5.17. The estimation of coral bleaching

is conducted using the highest SST difference occurred during La Niña temperature relative to mean SST from 1982 to 2008.

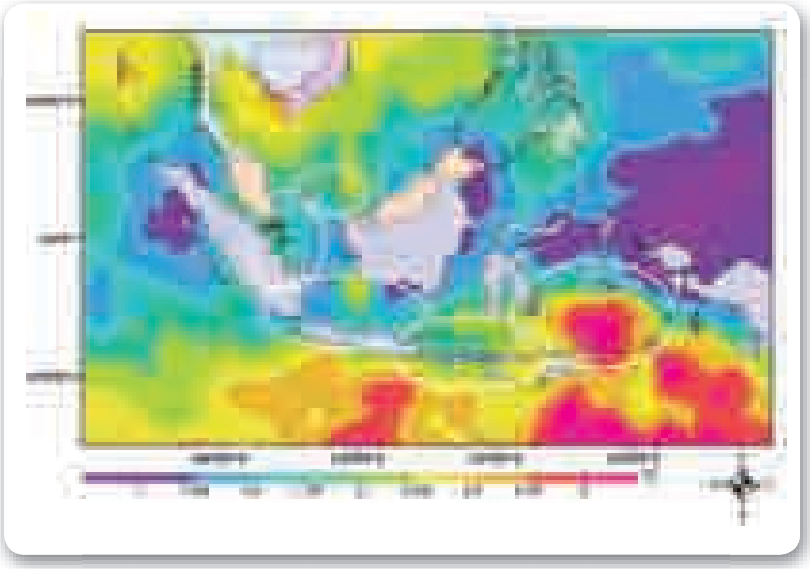

Figure 5. 17 Estimated locations where massive coral bleaching happens based on the difference of the highest sea level temperature to mean sea level temperature

Based on Figure 5.17, coral reef areas located in the southern equator are relatively more affected by the increasing of SST, and is suspected to suffer from massive bleaching, although there are reports of recovery processes in Kepulauan Seribu and Bali. However, this does not guarantee that in other areas, that suffered from severe bleaching with SST increase of more than 2.5°C, will also recovered. In addition, the projected increase of SST of 2°C until year 2100 will inhibit the recovery process of coral reef, and the rate of SST rise rate will exceeds the adaptation capacity of coral reef. Aside from the magnitude of SST rise rate, global warming also causes more frequent La Niña that may increase the abrupt changes of SST, which in turn will cause more stress to coral reef.

The rate of coral reef damage due to increasing SST during the La Niña events in 1998/1999 and 2006/2007 can be seen in Figure 5.18 below. The coral reef damage rate in 1998 is the highest on record and affected a vast area. After 1998, the damage rate is lower, but with higher frequency so that additional locations were subject to bleaching (Marshall and Schuttenberg, 2006). Aside from SST, coral reefs are also vulnerable to change in sunlight intensity. During calm wind and clear sky conditions, sunlight penetrates to 100 m depth, intensifying ocean heating and triggering coral bleaching.

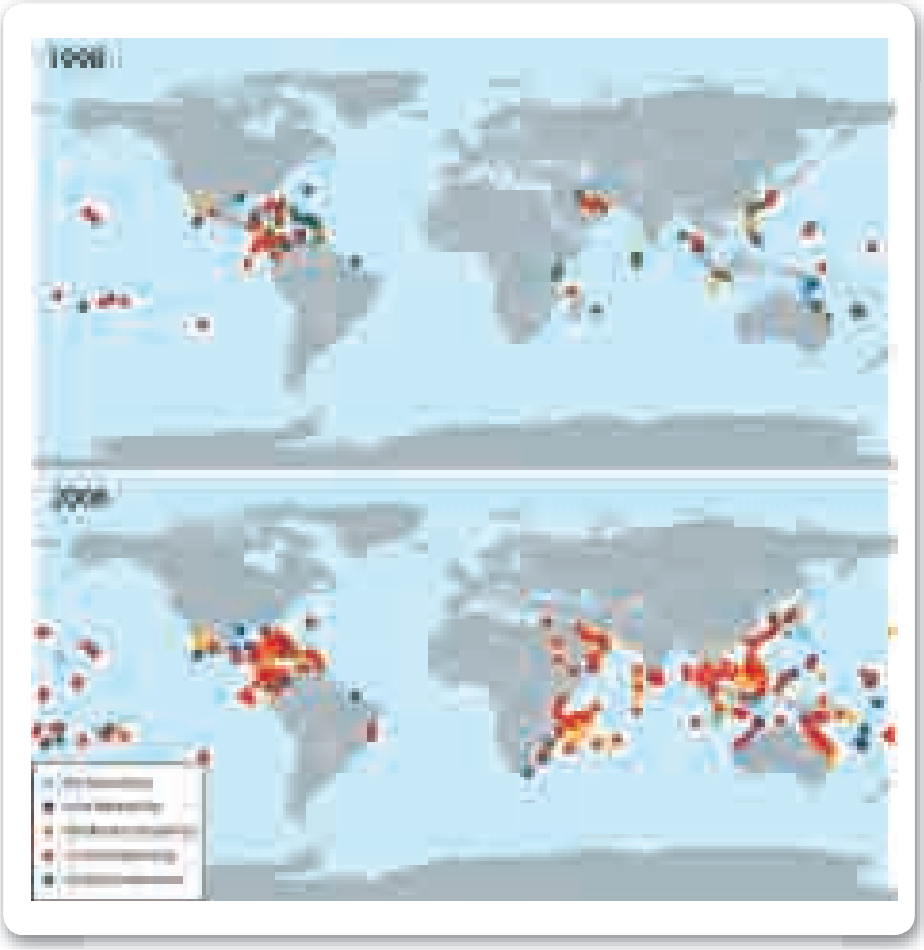

Figure 5. 18 Coral bleaching sites as a result of SST increase in 1998 until 2006 (Marshall and Schuttenberg, 2006)

The map of coral reef conditions in the Indonesian waters (based on data from *basereef.org*) are illustrated in Figure 5.19. This observation results indicated that massive coral reef damage has occurred in almost all of Indonesian waters, affecting vast areas. The coral reef condition in Indonesia in general is stressed and suffers bleaching in several areas, except in Papua and East Nusa Tenggara. By contrast, the coral reef along the southern coast of Java Island, although stressed, has not undergone high-intensity bleaching. This is because the SST trend in the area in recent years, tend to decrease even when this area has experienced SST abrupt change of more than 2.5°C. Finally, the management and monitoring of coral reef becomes much more urgent to prevent the massive coral reef bleaching.

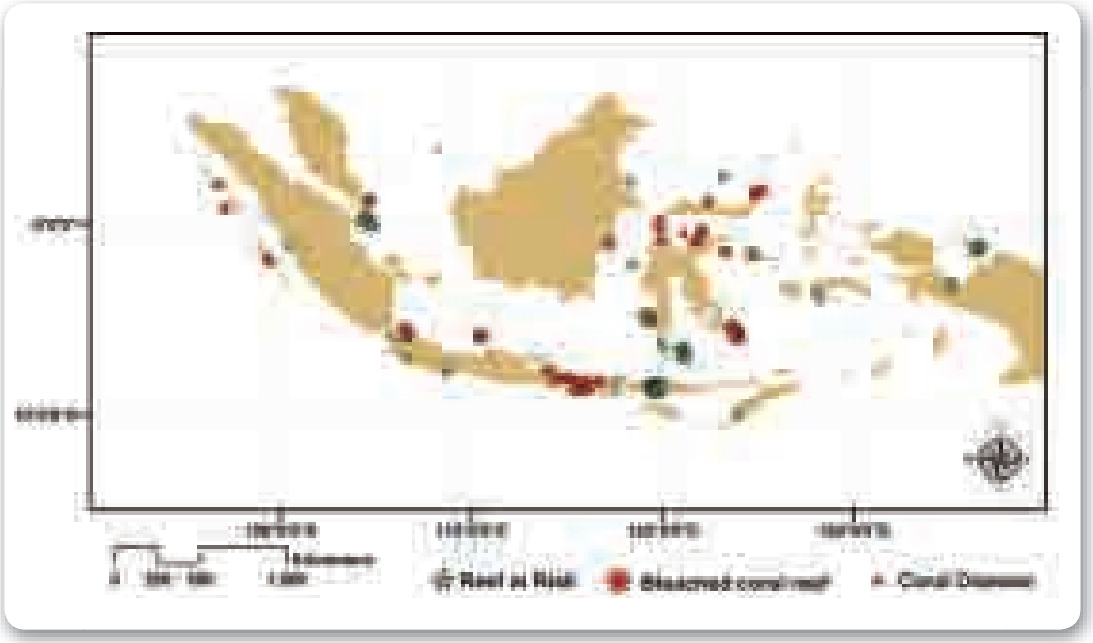

Figure 5. 19 Map of coral reef damage and coral bleaching based on data from basereef.org

6

ESTIMATION OF INUNDATED AREA

This chapter presents the projections of seawater submersion and coastal inundation in several major cities in Indonesia. These include Jakarta, Semarang, and Surabaya. Prediction of seawater submersion combines the projections of SLR under normal conditions, out to year 2100, with the projected magnitude of land subsidence, and the magnitude of tidal forcing during the highest tide.

6.1 Inundated Area Estimation

Generally, the estimation process to generate the map of coastal flooding and land inundation can be seen in Figure 6.1. Sea Level data projection is based on model, altimeter, and tidal data. In addition, the monthly highest tide data is based on modeling result from the Ocean Tidal Inverse Solutions model (OTIS).

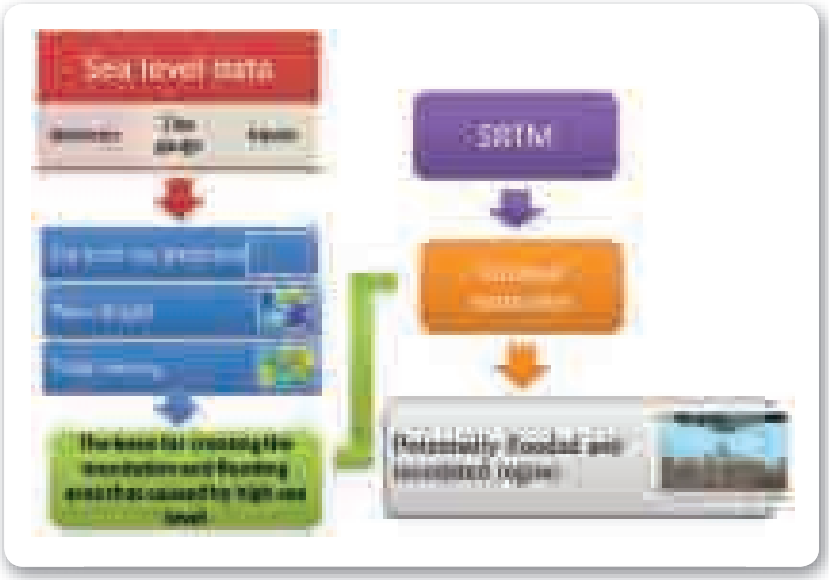

Figure 6. 1 Flow chart of process and general method for estimating sea-water-inundated area in year 2100

The projected sea level rise in Jakarta at year 2100 during high tide can be seen in Figure 6.2. The estimation of inundated area is based on data from Shuttle Radar for Topographic Mission (SRTM) by 30 m spatial resolution, and overlaid with satellite image data. The projected area of inundation incorporates (1) projections of subsidence level in Jakarta (which is approximately 3 cm/year according to Hirose et al., 2001); (2) the sea level rise estimation of 1 m/century; and (3) the influence of tides ranging from 80 cm up to 1 m. Based on the analysis of SRTM data, it can be seen that the inundated area due to the influence of sea level rise in Jakarta, is spread in almost all Jakarta's coastal zone, with wide coverage area. Almost all of North Jakarta area would be inundated by seawater, especially in the Muara Angke region, in Grogol, and in some areas of northern Menteng. Seawater inundation retreats the coastline by an amount ranging from 0 m up to 10 km. The vastness of inundation in coastal regions affects the lives of people all along the coast. The area of prawn ponds and agriculture fields area are certain to be reduced.

Figure 6. 2 Estimation of sea-water-inundated area in Jakarta due to influence of sea level rise which reach 1 m, subsidence level of 3 m per century, and 80 cm of tide. Area inside the polygon shows inundation area with altitude from 1m to 4m

Seawater infiltration is already increasing and it is estimated that it will soon reach the regions of South Jakarta. The sea level rise and the magnitude of subsidence level in Jakarta have caused flooding to widen over larger areas in the rainy season, spreading to almost all of Jakarta. This situation is complicated by the weakening river flow that is due to the decrease of altitudinal difference between the river and the sea level.

The influence of sea level rise in the Semarang region can be seen in Figure 6.3. The estimation of seawater inundation data incorporates the results of subsidence level analysis in Semarang (which is about 2 cm/year, according to Hirose et al., 2001); and an estimated sea level rise of 1 m/century; as well as the expected effects of a 50 cm rise in the height of high tide. Based on the analysis using SRTM data, we can see that the extent of the inundated area due to the influence of SLR extends over almost all of Semarang coast with vast coverage area. Almost all of northern Semarang would also be inundated by water. The same fate is likely to affect the sub-district of Tugu, some of West and Central Semarang and Genuk. In this case, the seawater inundation can be expected to reduce the coastline anywhere from 0 m to 6 km.

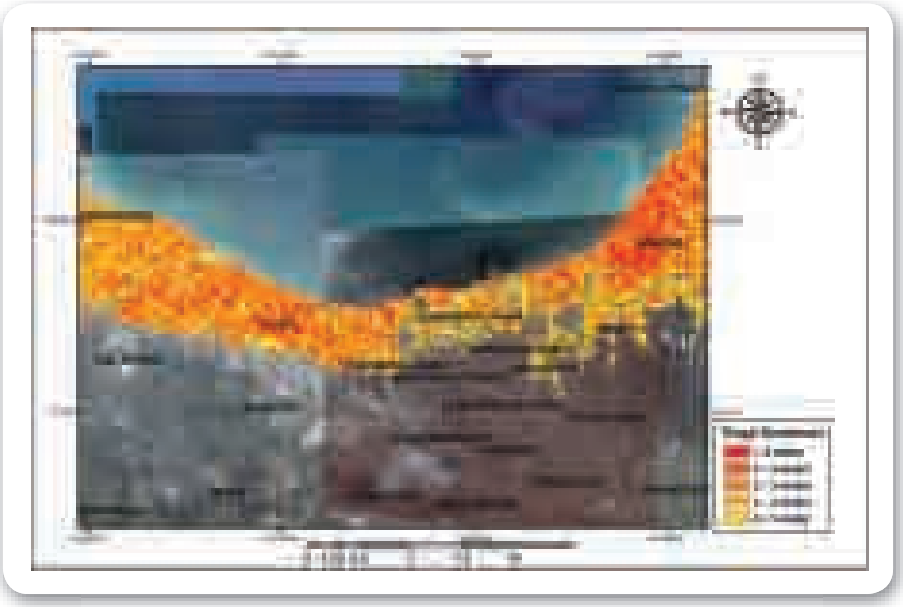

Figure 6. 3 Estimation of sea water-inundated area due to influence of sea level rise that reaches 1 m, subsidence level of 2 m per century, and 50 cm of tide. Area inside the polygon shows inundation area with altitude from 0m to 4m

The influence of sea level rise in Surabaya can be seen in Figure 6.4. Assuming that sea water-inundated area is determined by the estimated subsidence level in Surabaya of 2.5 cm per year, the estimated sea level rise magnitude is 1 m per century, and the effect of the highest monthly tidal increase is 1.5m, then water will inundated areas with elevation of 0 m up to 5 m. Based on the above assumptions, then this sea water inundation will further reduce the coastline anywhere from 0 m to 5 km. Included in the affected areas are the area of Kenjeran, Sukolilo and some regions of East Surabaya. Northern Surabaya, up to Pasar Turi Station, would be partially inundated when the sea level rise is more than 4 m. Sea water-inundated areas are widening along with the height of ocean waves during rainy season in January and the peak of the dry season in August, leading to a sea level rise estimation of 6 m. During high tide, area inundated by seawater is estimated to reach Gubeng. Residential areas, industrial areas, prawn ponds, and agriculture fields would all be reduced, severely hampering Surabaya's economy.

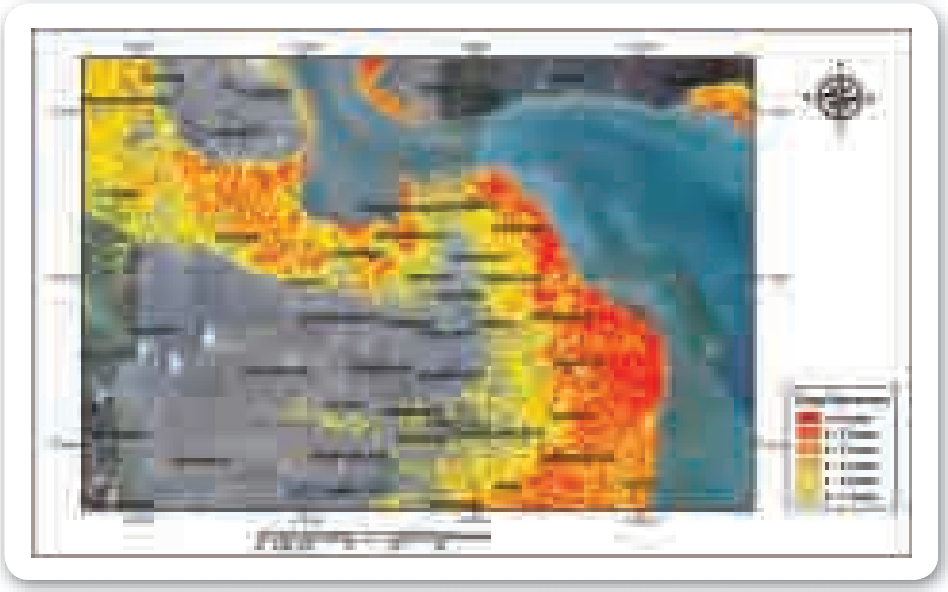

Figure 6. 4 Estimation of sea water-inundated area due to the influence of sea level rise that reaches 1 m, subsidence level of 2.5 m per century, with highest tide as high as 1.5 m from MSL. Area inside the polygon shows inundation area with altitude from 0 m to 5 m

6.2 Inundated Area Estimation during Extreme Weather Events

With global warming become more intensive, the frequency of ENSO occurrence is expected to increase. Future episodes of El Niño will be followed by the occurrence of La Niña. This transition period will cause abrupt sea level changes, which could reach up to 20 cm. Aside from the drastic increasing sea level, extreme climate conditions will trigger extreme weather events, which may cause additional high ocean waves. The magnitude and height of extreme waves happening in the Indonesian waters is discussed in Chapter V.

Based on the extreme weather analysis, relative sea level (including additional ocean wave height), compared with the conditions of sea level in year 2000, can be estimated mathematically as follows:

$$T_{EE}=M_{SL}+H_{EL}+H_{W}+H_{PS}+S_{L} \qquad (6\text{-}1)$$

Where T_{EE} is sea level during extreme weather, M_{SL} is average sea level in year 2100, H_{EL} is the increasing of sea level during the transition period between El Niño and La Niña, H_{W} is wave height, H_{PS} is the tidal level, and S_{L} is subsidence level.

From equation (6-1), the sea level in Jakarta during extreme weather events in year 2100 is likely to be between 7 m and 8 m, with M_{SL} =1 m, H_{EL}=20 cm, H_{W} =2.5 m, H_{PS}=80 cm, and S_{L} =3 m. Projections of sea-water-inundated areas in Jakarta are illustrated in Figure 6.5, and the inundated area in Semarang and Surabaya are shown in Figure 6.6 and Figure 6.7, respectively.

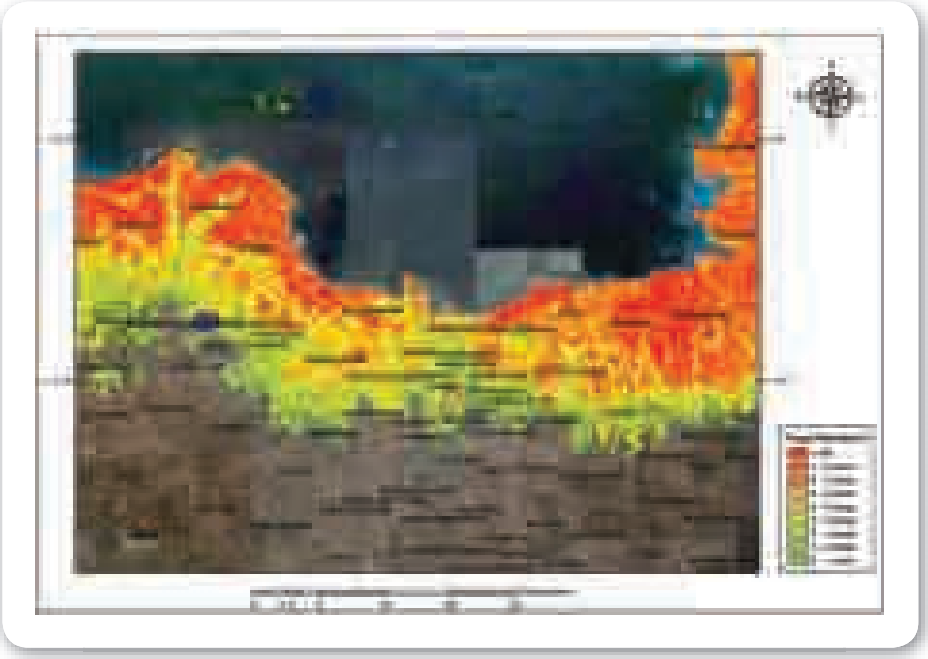

Figure 6. 5 Inundated area in Jakarta in year 2100 during extreme weather

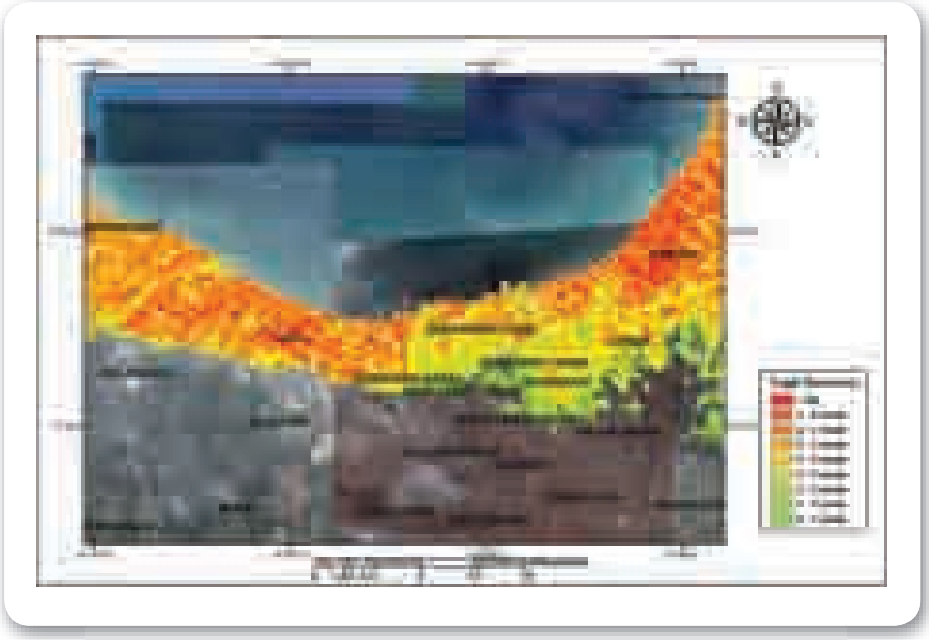

Figure 6. 6 Inundated area in Semarang in year 2100 during extreme weather

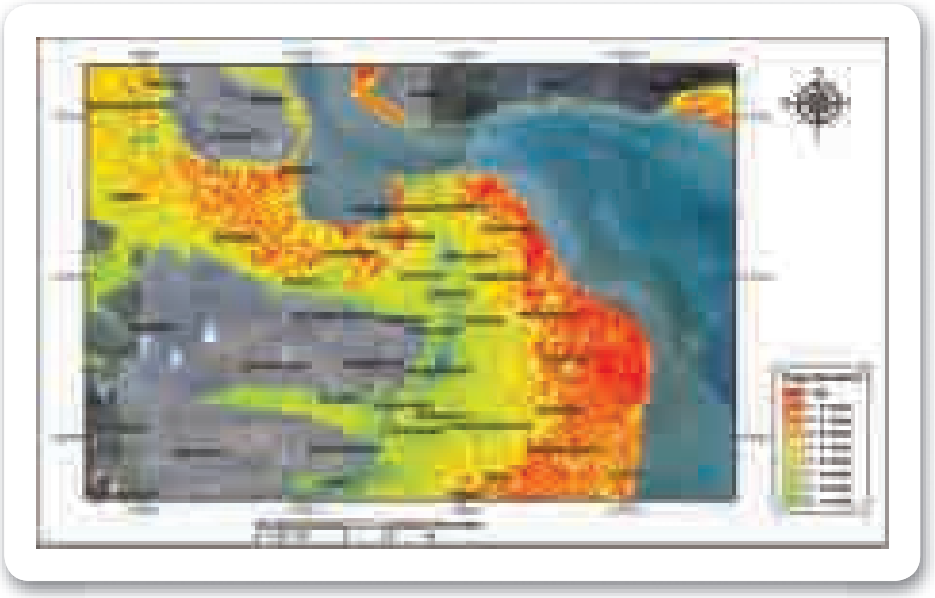

Figure 6. 7 Inundated area in Surabaya in year 2100 during extreme weather

Based on Figure 6.5 to Figure 6.7, the projected coastal flood in Jakarta, Semarang, and Surabaya will increase along with the widening of the inundated area and the reduction of the coastline by up to 15 km. The projected area of inundation in Jakarta spreads to Menteng, Gambir, and Setiabudi. Meanwhile, Soekarno-Hatta Airport will be completely inundated if the extreme wave height is 2m.

The projected area of inundation in Semarang does not change significantly, although the broadening of the affected area can still be seen compared to the inundation level without extreme waves. Meanwhile, the extent of inundated areas in Surabaya has a significant increase along with the broadening of the inundated area out to Wonokromo, Tegalsari and Sukomanunggal. It causes the coastline retreated by 10 km up to 20 km.

7

CONCLUSIONS AND RECOMMENDATIONS

Based on the analysis and study of the impact of global warming on sea level, SST, and climate variability such as El Nino and La Nina, we conclude that:

1. Based on observational data, the average SST rise rate in the Indonesian waters is ranging from 0.02°C to 0.023°C per year over the last century. Therefore, it can be concluded that, if the current trends continue, the SST rise until 2030 will reach 0.6°C to 0.7°C, and will reach 1°C to 1.2°C in 2050, compared to the one in 2000. Furthermore, SST will rise 1.6°C to 1.8°C in 2080, and the increase of temperature will reach 2°C to 2.3°C in 2100. Estimations from models have given the same results as observational data, although the model-estimated SST rise rate tends to be higher, with a lower range between the highest and lowest trends, a range of approximately 0.07°C per year.

2. Analysis results using altimeter data show that sea level rise rate is ranging from 0.2 cm/year to 1 cm/year, with an average rate of 0.6cm/year. The highest sea level rise occurs in the Pacific Ocean north of Papua, with an estimated rate of 1 cm/year. The lowest increase occurs along the southern coast of Java and ranges from only 0.2 cm/year to 0.4cm/year. The rise of sea level in 2030 will reach 6 cm to 30 cm, with an average increase for the whole of Indonesia ranging from 15 cm to 18 cm. In 2050, sea level could increase by 10 cm to 50 cm with an average increase of 25 cm to 30 cm. The increase of sea level in 2080 is expected to reach about 16 cm to 80 cm, with an average increase ranging from 40cm to 48cm. Eventually, sea level will increase by 20 cm to 100 cm, with an average increase of 50 cm to 60 cm in 2100.

3. Based on tidal gauge data, the projected sea level rise in 2030 is estimated to reach 24 cm ±16 cm, relative to the sea level in 2000. Following this, due to the rise of SST, sea level rise will reach 40 cm ±20 cm and 56 ±32 cm in 2050 and 2080, respectively. Eventually, sea level is projected to rise by 80 cm ±40 cm in 2100.

4. The IPCC model estimates that the rate of sea level rise ranges between 0.7 cm/year and 0.8 cm/year. Thus, sea level would be expected to rise by 22.5 cm ±1.5 cm in 2030 relative to sea level in 2000, and will later range between 35 cm up to 40 cm in 2050. Sea level will continuously increase and reach 56 cm to 60 cm ±4 cm in 2080, and 75 ±5 cm in 2100.

5. Based on research since 2006 that incorporates the dynamics of ice mass change and the ice melting in the Greenland and Antarctica, it is estimated that the sea level rise will reach 175 cm in 2100 relative to sea level in 2000. Sea level in 2030 will rise 52.5 cm, in 2050 will rise 87.5 cm, and will rise 140 cm in 2080. This strong increase in sea level may cause more abrasion, erosion, and seawater inundation, not only because of sea level rise, but also due to the combined effects of storm waves, tidal forcing, and extreme events such as La Nina, which are modulated by the high sea level.

6. Analysis of extreme events, namely ENSO, up to year 2100 that incorporates sea surface temperatures in the Nino3 region, shows an increase of frequency of ENSO from once every three to seven years, to once every two years.

7. When El Niño occurs, sea level will be depressed by up to 20 cm below normal, and during the La Niña period, regional sea level will be elevated by 10 cm to 20 cm. This affects the risks of flooding, abrasion, and seawater intrusion, especially during La Niña, which brings higher rainfall intensity.

8. The rise of sea levels and the land subsidence in Jakarta, Semarang, and Surabaya, will cause flooding in regions with an elevation between 0 m to 3 m, 0 m to 4 m, and 0 m to 5 m in 2100. Generally, the northern coastline of Java will be eroded and reduced by anywhere from 0 km to 20 km. As the impact of intensified extreme weather, flooded areas will spread and the depth of flooding will increase up to 3 m to 4 m.

9. Coral reefs are very vulnerable to abrupt temperature changes. Generally, coral reefs can survive well in temperatures of 26°C to 30°C. The rise of ocean temperatures of 1°C to 2°C from the historical yearly average can take the local environment out of this "safe" range and can trigger coral bleaching.

10. La Niña and El Niño cause tidal waves with variations between 2.1 m to 5 m, even though El Niño does not have a significant effect on wave heights in the Indian Ocean. The high ocean waves during the El Niño and La Niña phases will increase the intensity of coastal erosion and abrasion, with greater onshore destruction. In the end, with the higher intensity of El Niño and La Niña, these dynamic may cause more extensive damage to coastlines, even though the increase rate of sea water levels remains only 1 cm/year in the short term.

The sea level rise projections show a different results among the analysis based on tidal gauge, altimeter and model-estimated data. However, the sea level rise is a certainty. This discrepancy maybe addressed to the uncertainty of sea level in 2100, ranging from 40cm to 150cm.

The adaptation to global warming and climate change on the marine sector should be conducted by strengthening the integrated research and monitoring not only limited to the physical aspects, but also on the marine and coastal ecosystems. Based on the high uncertainty of global warming and climate change impacts on the marine sector, the numerical models are only suitable to analyze the impact of climate change in short and medium-term predictions. An integrated model of physical aspects, biology and ecosystems such as ROMS (Regional Ocean Modeling System) may be one method for analyzing the impact of climate change on the ocean including sea level, ocean wave, current patterns, temperature, salinity, water and sediment transports and biogeochemical aspects such as carbon and nitrogen fluxes.

In addition, based on these conclusions, the adaptations recommended on reducing the effect of global warming on the ocean and coastal sectors can be described as follows:

1. Improving human resources and institutional capacity through education, skills training, and experience in managing coastal areas and wetlands.
2. Developing improved management of coastal ecology, comprising the conservation of coastlines, wetlands, etc.
3. Strengthening the Disaster Warning System (DWS) in anticipation of tidal waves and storm surges, especially in terms of their impacts on the transportation sector.
4. Strengthening the management of the coastal zone by improving the accuracy of available data, such as sea levels and extreme events (floods and tidal waves), so that these data can be used to monitor continuously the impact of global warming.
5. Constructing buildings so as to break waves, or planting mangroves to decrease the effect of global warming on coastal zones.
6. Monitoring coral reef damage using daily global SST data through the coral reef watch.

REFERENCES

Bamber J.L., R.L. Layberry, and S.P. Gogenini, 2001, A new ice thickness and bedrock data set for the Greenland ice sheet, JGR Atmospheres, 106, D24: 33773-33780.

Bindoff, N.L., Solomon, S., D. Qin, M. Manning, Z. Chen, M. Marquis, K.B. Averyt, M. Tignor, and H.L. Miller, 2007: Observations: Oceanic climate change and sea level. In: Climate Change 2007: The Physical Science Basis. Contribution of Working Group I to the Fourth Assessment Report of the Intergovernmental Panel on Climate Change. Cambridge University Press, Cambridge, United Kingdom, 385-432.

Coles, S. L., and B.E. Brown, 2003, Coral bleaching—capacity for acclimatization and adaptation, J. Adv. Mar. Bio., Vol. 86, 183-223.

Egbert, G. D., A. F. Bennett, and M. G. G. Foreman, 1994: TOPEX/Poseidon tides estimated using a global inverse model. J. Geophys. Res., 99, 24 821–24 852.

Folland, C.K., N.A. Rayner, S.J. Brown, T.M. Smith, S.S.P. Shen, D.E. Parker, I. Macadam, P.D. Jones, R.N. Jones, N. Nicholls and D.M.H. Sexton (2001). "Global temperature change and its uncertainties since 1861". Geophysical Research Letters 28: 2621-2624.

Hendiarti, N, Suwarsono, K. Amri, E. Aldrian, R. Andiastututi, S. I. Sachoemar, and I. B. Wahyono, 2005, Seasonal Variation of Pelagic Fish Catch around Java, Oceanography, Vol. 18, No. 4, 112-123.

Hirose, K., Y. Maruyama, D. Murdohardono, A. Effendi, H. Z. Abidin, 2001, Land subsidence detection using JERS-1 SAR Interferometry, 22nd Asian Conference on Remote Sensing, 5-9 November 2001.

Hoegh-Guldberg, O., 1999, Climate change: coral bleaching and the future of the world's coral reefs, J. Mar. and Fresh. Res., Vol. 50, pp. 839-866.

Intergovernmental Panel on Climate Change, 2007, Climate Change 2007 - The Physical Science Basis: Contribution of Working Group I to the Fourth Assessment Report of the IPCC. Cambridge, Cambridge University Press.

Knutti, Reto and T. F. Stocker, 2000, Influence of the Thermohaline Circulation on Projected Sea Level Rise, Journal of Climate 13, 12: 1997-2001.

Lythe, B. Matthew, D. G. Vaughan and the BEDMAP Consortium, 2001, BEDMAP: A new ice thickness and subglacial topographic model of Antarctica, J. Geo. Res. 106, B6: 11335–11351.

Marshall, P., and H. Shuttenberg, 2006, A Reefs Manager's Guide to Coral Bleaching, Great Barrier Reef Marine Park Authority, 1-166 pp.

Meehl, G. A., Solomon, S., D. Qin, M. Manning, Z. Chen, M. Marquis, K.B. Averyt, M. Tignor, and H.L.

Miller in: Climate Change 2007: The Physical Science Basis. Contribution of Working Group I to the Fourth Assessment Report of the Intergovernmental Panel on Climate Change, Cambridge University Press, Cambridge, United Kingdom, 748-845.

Rahmstorf, S., 2007: A semi-empirical approach to projecting future sea-level rise. Science, 315, 368-370.

Rayner, N. A., D. E. Parker, E. B. Horton, C. K. Folland, L. V. Alexander, and D. P. Rowell, 2003, Global analyses of sea surface temperature, sea ice, and night marine air temperature since the late nineteenth century, J. Geph. Res., VOL. 108, NO. D14, 4407.

Ridley, J.K., P. Huybrechts, J.M. Gregory, and J.A. Lowe, 2005: Elimination of the Greenland ice sheet in a high CO2 climate. Journal of Climate, Vol 18, 3409-3427.

Rignot, Eric and P. Kanagaratnam, 2006, Changes in the Velocity Structure of the Greenland Ice Sheet, Science, 311, 5763: 986-990.

Small, C., and R.J. Nicholls, 2003: A global analysis of human settlement in coastal zones. J. Coastal Res., 19, 584-599.

Steffen, K., P. U. Clark., J. G. Cogley, D. Holland, S. Marshall, E. Rignot, and R. Thomas, 2009, Rapid Changes in Glaciers and Ice Sheets and their Impacts on Sea Level in: Abrupt Climate Change, Final Report, Synthesis and Assessment Product 3.4, U. S. Geological Survey.

Sofian, I, Kozai, K, and Ohsawa, T (2008), "Investigation on the relationship between wind-induced volume transport and mean sea level in the Java Sea using an oceanic general circulation model" Journal of Marine and Meteorological Society of Japan, Umitosora, Volume 84

Sofian, I and A.B. Wijanarto (2008) "Kenaikan Tinggi Muka Laut di Jakarta berdasarkan IPCC AR4", Jurnal Geomatika, Vol. 14, No. 2, pp. 71-80.

Sofian, I (2007), "Simulation of the Java Sea using an Oceanic General Circulation Model", Jurnal Geomatika, Vol. 13 No. 2, pp. 1-14.

Timmermann, A., M. Latif, A. Bacher, J. Oberhuber, E. Roeckner, 1999, Increased El-Niño, Nature, 398, 694-696.

Timmermann, A., 2001, Changes of ENSO stability due to Greenhouse Warming, Geophysical Research Letters, 28, 8: 2064-2066.

Torrence, C. and G. P. Compo., 1999, A Practical Guide to Wavelet Analysis, Bulletin of the American Meteorological Society, 79, 1:61–78.